Journal Name

ARTICLE

Two-dimensional materials for miniaturized energy storage devices: from individual devices to smart integrated systems

Received 00th January 20xx,
Accepted 00th January 20xx

DOI: 10.1039/x0xx00000x

www.rsc.org/

Panpan Zhang,‡ Faxing Wang,‡ Minghao Yu, Xiaodong Zhuang* and Xinliang Feng*

Nowadays, the increasing requirements of portable, implantable, and wearable electronics have greatly stimulated the development of miniaturized energy storage devices (MESDs). Electrochemically active materials and microfabrication techniques are two indispensable parts in MESDs. Particularly, the architecture design of microelectrode arrays is beneficial to the accessibility of two-dimensional (2D) active materials. Therefore, this study reviews the recent advancements in microbatteries and microsupercapacitors based on electrochemically active 2D materials. Emerging microfabrication strategies enable the precise control over the thickness, homogeneity, structure, and dimension in miniaturized devices, which offer tremendous opportunities for achieving both high energy and power densities. Furthermore, smart functions and integrated systems are discussed in detail in light of the emergence of intelligent and interactive modes. Finally, future developments, opportunities, and urgent challenges related to 2D materials, device fabrications, smart responsive designs, and microdevice integrations are provided.

1. Introduction

Energy production using scarce fossil fuels such as coal, petroleum, and natural gas is causing severe economic and environmental issues worldwide. There is an urgent need to exploit renewable resources such as solar, wind, tidal, and geothermal energy. However, owing to the intermittency of these natural resources, energy storage systems play an important role in storing the electricity generated from them.[1-4] Among diverse storage media, electrochemical energy storage devices, comprising rechargeable batteries (RBs) and supercapacitors (SCs), are widely used in portable electronics (*e.g.*, mobile devices, multimedia players, and personal medical devices), medium transportation systems (*e.g.*, electrical vehicles and aerospace), and large-scale energy storage systems (*e.g.*, electric grids).[5-9]

RBs and SCs are similar in that they have a positive electrode, a negative electrode, a separator, and an electrolyte.[10, 11] However, they have different charge-storage mechanisms. As shown in Fig. 1a, SCs are usually classified as electric double-layer capacitors (EDLCs) and pseudocapacitors.[12-20] In EDLCs, electrostatic charge accumulates at the electrode/electrolyte interface through ion adsorption to form electric double layers. In pseudocapacitors, charge is stored using reversible surface/near-surface Faradic reactions. In general, SCs provide fast charge/discharge capability (high power density) because of surface-mediated ion diffusion. RBs rely on reversible redox reactions on the surfaces and in the bulk form of active materials for charge storage (Fig. 1b). As a result, RBs have much higher energy densities, but they suffer from insufficient power density ascribed to the slow ion diffusion kinetics in solid electrode materials.[21-23] High-efficiency energy storage applications require these devices to be compact and to yet store and release large amounts of electrical energy rapidly. Doing so would be impossible without selecting appropriate electrode materials and designing suitable device configurations.

In recent years, the development of portable, implantable, and wearable electronics has focused on the miniaturization, low weight, safe, long-term, and high-speed operation, thus further stimulating the demand for miniaturized energy storage devices (MESDs).[24, 25] Undoubtedly, to collect, receive, and transmit signals, these microelectronics must be connected with power sources. Furthermore, practical needs have resulted in an increasing demand for self-powered integrated systems that can operate sustainably and independently without maintenance. Energy can be extracted and converted into electricity by energy harvesters based on piezoelectric, triboelectric, thermoelectric, and photovoltaic effects. In this regard, MESDs are highly desirable to compensate for their intermittency and ensure long-term energy supply. Thus, MESDs such as microsupercapacitors (MSCs)[26-29] and microbatteries (MBs)[30-33] can be integrated with energy harvesting microsystems, achieving high peak power, long lifetime, and high rate capability while retaining reasonable energy density for practical applications in microsized integrated systems.[34] Fig. 1c shows a year-wise graph of publications reflecting the increasing research interests in MESDs. In addition, advanced microelectronics techniques provide a solid foundation for fabricating MESDs. Thus far, three

Department of Chemistry and Food Chemistry & Center for Advancing Electronics Dresden (cfaed), Technische Universität Dresden, 01062 Dresden, Germany. E-mail: xiaodong.zhuang@tu-dresden.de; xinliang.feng@tu-dresden.de
‡ These authors contributed equally to this work.

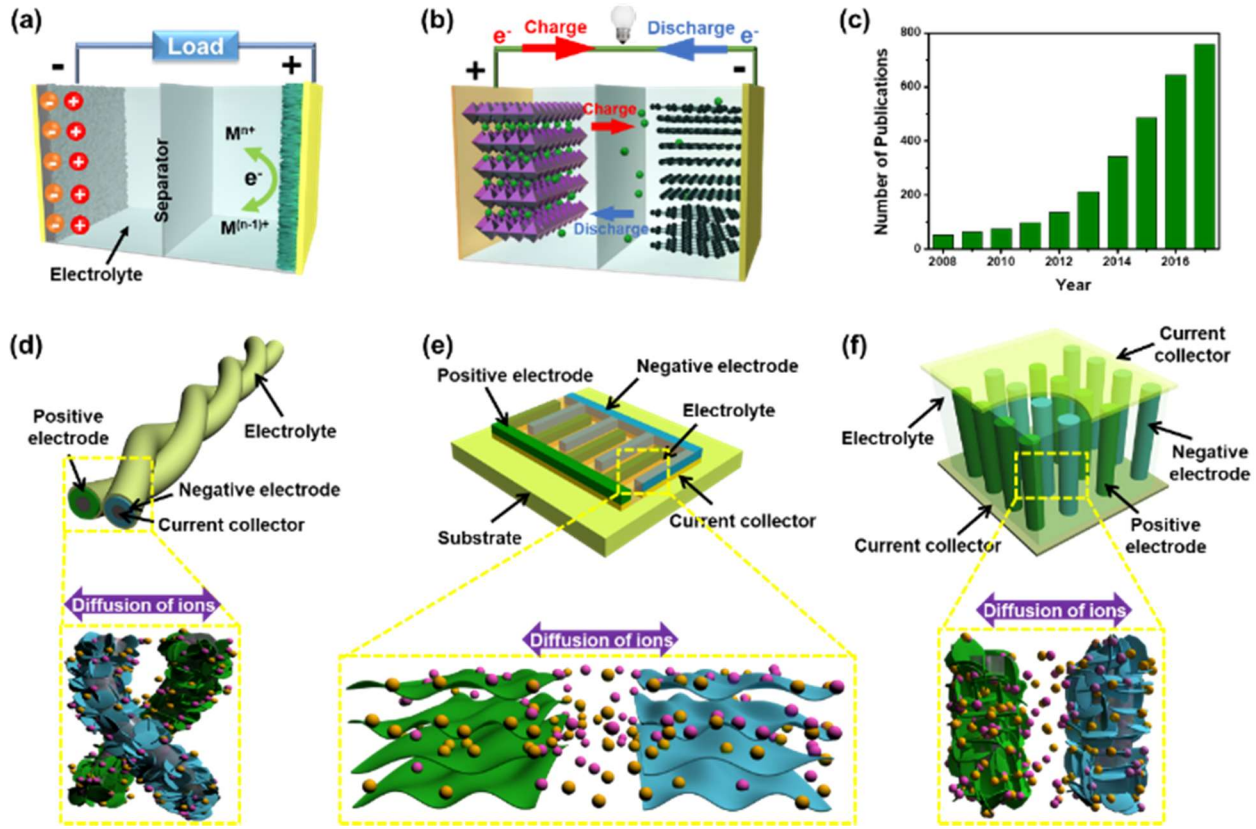

Fig. 1 (a) Schematic of charge storage *via* the ion adsorption/desorption of EDLC and redox reaction of pseudocapacitive material in an asymmetric supercapacitor. (b) Schematic of charge-storage mechanism in a typical RB by crystallographic phase transformation that occurs during the charge transfer processes. (c) Increasing trend in annual number of publications on MESDs during the last decade (2008–2017) using the keyword of "micro energy storage" as searched using SciFinder Scholar on January 15, 2018. Schematics of MESDs with different configurations based on electrochemically active 2D materials: (d) fiber shape, (e) in-plane architecture, and (f) 3D type.

main kinds of device configurations for MESDs have been established: fiber shape (Fig. 1d), in-plane architecture (Fig. 1e), and three-dimensional (3D) type (Fig. 1f).

To satisfy the ever-growing demands for electricity storage in both stationary and mobile electronic devices, advanced electrode materials must be developed for MESDs with both high energy and power densities. Two-dimensional (2D) materials represent an emerging class of materials with strong in-plane chemical bonding, but weak out-of-plane van der Waals interactions.[35] Such unique structure allows the manipulation of the interlayer space through efficient and effective nanoscale engineering. Since the discovery of monolayer graphene exfoliated from graphite in 2004,[36] 2D materials have undergone rapid development for applications of their unusual electronic, mechanical, chemical, electrochemical and optical properties. Like graphene, many 2D materials exhibit large planar topology (>100 nm) and ultralow thickness (single- or few-atom thickness). Extensive studies have been conducted on 2D materials with diversified applications, including electronics, superconductors, sensing, catalysis, energy storage and energy conversion, *etc.*[37-41] Particularly, atomic-scale ultrathin layered structures of electrochemically active 2D materials are attractive for MESDs. The exposed surface area of 2D materials opens 2D channels for fast ion transport and shortens the charge transport path. Furthermore, the distance between microelectrodes downs to micron level, effectively shortening the diffusion paths of ions in electrolyte and microelectrodes. Typical 2D materials for MESDs include transition metal dichalcogenides (TMDs), transition metal oxides (TMOs)/hydroxides (TMHs), transition metal carbides/nitrides (mainly MXene materials), and 2D metal-organic frameworks and covalent-organic frameworks (MOFs and COFs). Thus far, considerable attentions have been focused on engineering these 2D materials structurally to enhance their electrochemical performances.[42-44]

Several recent reviews on MESDs have mostly focused on issues such as electrode materials, fabrication methods, or device design for certain device types such as fiber-shape MSCs,[45, 46] in-plane MSCs,[47] and 3D MBs.[8, 48] However, no systematic summary has been provided for recent progress in the development of next-generation miniaturized MESDs for smart integrated systems based on 2D materials, including emerging fabrication technologies, introduction of smart functions, and device innovations for system integrations. Toward this end, the current review article aims at a comprehensive description of the latest scientific progresses towards MESDs using 2D materials from individual devices to smart integrated systems (Fig. 2). First, we describe the recent development of MESDs, including MSCs and MBs, according to the representative 2D materials and prominent fabrication techniques. This section addresses the relationship between fabrication strategies and corresponding electrochemical

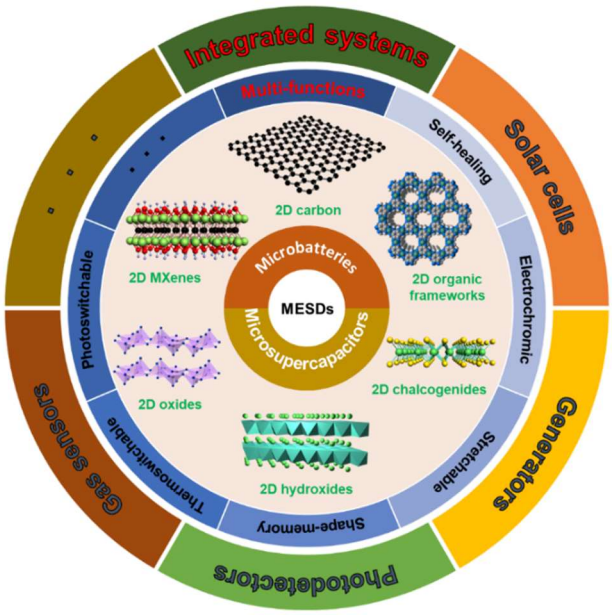

properties. Afterwards, we discuss novel strategies to introduce stimulus–response functions into MESDs, with a particular focus on their design principles and special functional properties. We further demonstrate the state-of-the-art research in the area of integrated systems, especially the integration of MESDs with solar cells, nanogenerators, photodetectors, and gas sensors. Finally, we outline the future developments, prospects, and key technological challenges based on the considerations of performance improvement, smart responsive design, and microdevice integration using 2D materials.

Fig. 2 Schematic of current review content including electrochemically active 2D materials, fabrication technologies, functional responses, and smart integrated systems.

2. MESDs

MESDs offer robust power delivery, making them useful in wireless sensor networks for home automation, transport surveillance, health control, environmental monitoring, and industrial process tracking. Micropower systems can be fabricated with micrometer-scale lengths and improved performance compared to conventional sandwich-structured energy storage devices that is attributable to short ion/electron diffusion lengths. Moreover, miniaturized devices accelerate both ion and electron transports within electrochemically active 2D materials and reduce the resistance across the positive electrode, negative electrode, and electrolyte.[49] This section particularly discusses the MESDs employing various microfabrication methodologies based on suitable 2D materials.

2.1. MBs

Commercial RBs in the form of cylindrical or coin devices are incompatible with miniaturized autonomous device systems. Instead, MBs are more suitable for meeting the geometrical requirements of microelectronics. 2D materials have already displayed fascinating properties in MBs including good mechanical flexibility, short ion diffusion lengths, and a large exposed surface for redox reactions.[50-53] In the following part, we will discuss the recent developments in MBs based on 2D cathode and anode materials.

2.1.1 2D cathode materials

2D cathode materials including 2D intercalation compounds (like $LiCoO_2$ nanosheets), 2D TMOs (like V_2O_5 nanosheets), 2D conductive polymer nanosheets (such as polypyrrole), 2D MOFs, graphene-related composites, *etc.*, have been reported for RBs.[52, 54-57] Nevertheless, due to the complex microelectrode fabrication methods and packaging technologies, there are only scarce examples of 2D cathode materials for MBs, which mainly involve graphene-based composites and graphene itself. For the graphene-based composite, graphene usually serves as the electron conducting additives for fabricating microelectrodes due to its extremely high surface/mass ratio, excellent flexibility and high electrical conductivity; while graphene itself can serve as an active cathode material for anion storage in MBs.

In 2016, Hu *et al.* demonstrated a 3D printed interdigital MBs using a highly viscous graphene inks containing $LiFePO_4$ cathode.[33] Specifically, a typical concentrated graphene oxide (GO) ink (80 mg mL^{-1}) containing the $LiFePO_4$ cathode with high viscosity and optimum viscoelastic properties was layer-by-layer (LBL) printed and then arranged into an interdigital pattern using an extrusion-based 3D printing technique. The printed GO based electrodes were then freeze-dried for removing the water and thermally annealed for reduction and improvement of the electrical conductivity. The resultant 3D-printed $LiFePO_4$/graphene cathode exhibited a specific capacity of 160 mAh g^{-1}, approaching to the theoretical capacity of $LiFePO_4$.[33] The achieved value was much higher than those $LiFePO_4$ cathodes using conventional carbon additives such as carbon black. Apart from the improvement of conductivity and specific capacity, graphene could effectively accommodate the volume expansion of electrode materials, leading to a markedly improved cycling performance. In addition, the construction of hierarchically porous graphene as conducting additives for loading active materials is favorable for the easy diffusion of electrolytes and fast kinetic of electrochemical reactions in MBs.

Different from the above case, few-layer graphene reversibly accommodates anions (PF_6^-, ClO_4^-, BF_4^-, *etc.*) at high voltages, which can thus be used as a cathode material for MBs.[58, 59] Because there was a large voltage difference in few-layer graphene for anion and cation storage, our group recently reported a dual-ion MB based on interdigital graphene electrodes with a thickness of ~50 μm through a simple spray-coating technology (Fig. 3a). The quantity and density of graphene based microelectrodes could be controlled by adjusting the aqueous dispersion concentration of the electrochemically exfoliated graphene and spray-coating time. The fabricated dual-ion MBs exhibited a maximum areal capacity of 35 μAh cm^{-2} (Fig. 3b), which was comparable to those of $LiCoO_2$-based thin-film MBs. Notably, for the PF_6^- intercalation into few-layer graphene cathode, there was a high

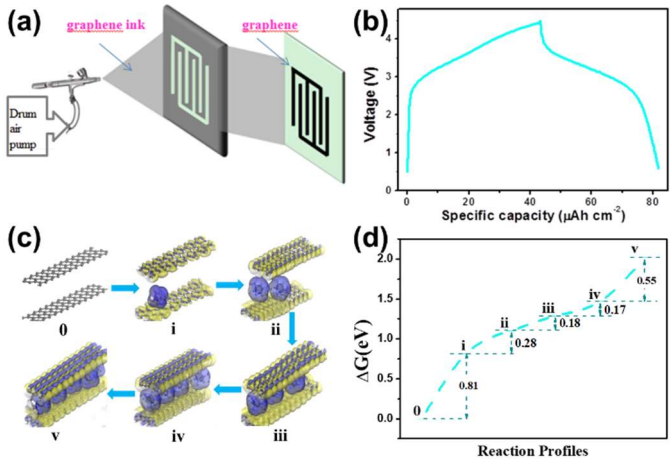

Fig. 3 The dual-ion MB based on few-layer graphene. (a) Schematic illustration of the fabrication of the dual-ion MB in-plane configuration. (b) GCD curves. DFT calculation for (c) the reaction profiles of anion transport across the two-layer graphene and (d) the corresponding energies at each step. Reproduced with permission.[58] Copyright 2017, John Wiley & Sons, Inc.

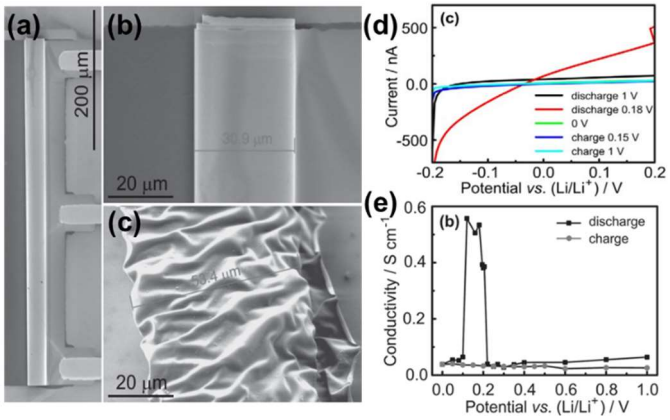

Fig. 4 The MB based on the Si nanomembrane and the *in-situ* probing of electrical conductivity of Si nanomembranes during lithiation/delithiation redox reactions. (a, b) SEM images of the single-microtube-MB fabrication from the Si nanomembranes before cycling and (c) after 3 cycles. (d) The current and (e) electrical conductivity at different discharge/charge states for the Si nanomembrane in the single-microtube-MB. Reproduced with permission.[65] Copyright 2014, John Wiley & Sons, Inc.

irreversible capacity loss in the initial cycles. Such kind of irreversible capacity loss in the initial cycles usually does not happen in other cathode materials (like $LiMn_2O_4$ and $LiFePO_4$) for Li-ion storage. Moreover, the initial charging process of the graphene based dual-ion MBs started at a higher voltage than that of the ongoing cycles. Presumably, there was an "activation" process during the first charge/discharge cycle in graphene electrode, which was further demonstrated by the density functional theory (DFT) calculation for the reaction profiles of anion transport across the graphene layers (Fig. 3c). The calculated energy barrier of the initial anion intercalation was much higher than those of the subsequent anion intercalations (Fig. 3d), suggesting that initial anions (PF_6^-) were required to widen the graphene interlayer gaps at the electrode/electrolyte interface. Furthermore, the widen graphene layers after the initial anion intercalation enabled the following anions to intercalate more easily.[58] Currently, one major challenge of dual-ion MBs is the low volumetric energy density compared with commercial Li thin-film MBs. The theoretical specific capacity of the few-layer graphene (or graphite) cathode materials was relatively low (less than 125 mA h g^{-1} for $C_{18}PF_6$), which could not meet the ever-growing high-energy-density demand for their widespread applications.

2.1.2 2D anode materials

Because of the low redox potentials and ultrahigh specific capacities, a lot of van der Waals 2D materials have been explored as anode materials for RBs, such as TMD, MXene, graphene, germanane, and antimonene.[43, 60-63] However, similar to 2D cathode materials for MBs, there are only a few examples about 2D anode materials until recently, including MoS_2 nanosheet and Si nanomembrane.

MoS_2, as one of the most studied TMDs, is a highly attractive 2D anode material for MBs due to its large theoretical capacity (up to 670 mAh g^{-1}). It possesses a layered structure with the weak van der Waals bonds between S–Mo–S layers. The interlayer spacing is 0.62 nm, which is beneficial for the intercalation of alkali metal ions. Nevertheless, the intrinsically low electrical conductivity due to its large band gap and large volume variation associated with a conversion mechanism usually lead to poor cycling stability and inferior rate capability. To address these issues, researchers constructed graphene-MoS_2 hybrids as electrode materials for MBs. In 2014, Cui *et al.* demonstrated graphene nanosheets as good substrates for the growth of vertically aligned MoS_2 sheets using a chemical vapor deposition (CVD) method.[64] The free of dangling bonds underlying graphene, such as boundaries and oxygen functional groups, could serve as nucleation sites for the van der Waals epitaxy of intermediate (MoO_{3-x}) of MoS_2. When the nuclei were formed, the MoO_{3-x} crystals could grow along the vertical direction, producing vertical MoS_2 sheets. As the result, the fabricated Li thin-film MB delivered an outstanding long-life cycling stability with a high areal capacity of 0.1 mAh cm^{-2} even after 1000 cycles, which was much better than the thin-film devices based on metal oxides (less than 100 cycles).[64] In addition, compared with compact thin-film structure, the vertical designing of the thin-film electrode could offer more reaction sites for the electrolyte ions and facile accommodation of the strains over repeated cycles.

Apart from MoS_2 anode, the Si anode based on the alloying/dealloying reaction is a promising anode for MBs owing to its extremely high specific capacities (lithiated to $Li_{4.4}Si$ with a theoretical capacity of 4200 mAh g^{-1}), low working voltages, and natural abundances. Nevertheless, the huge volume change (>300%) during the lithiation/delithiation process poses a big challenge for the application of Si anodes, which may cause the electrode pulverization and capacity fade during cycles. In 2014, Schmidt *et al.* demonstrated that designing 2D structure in Si anode could alleviate the large volume change during electrochemical processes.[65] A lab-on-chip MB with a single Si electrode derived from a 2D Si nanomembrane was assembled after infiltrating the liquid electrolyte and Li foil (Fig. 4a). Before lithiation, the Si nanomembrane had a smooth surface (Fig. 4b). After three cycles of lithiation/delithiation, the

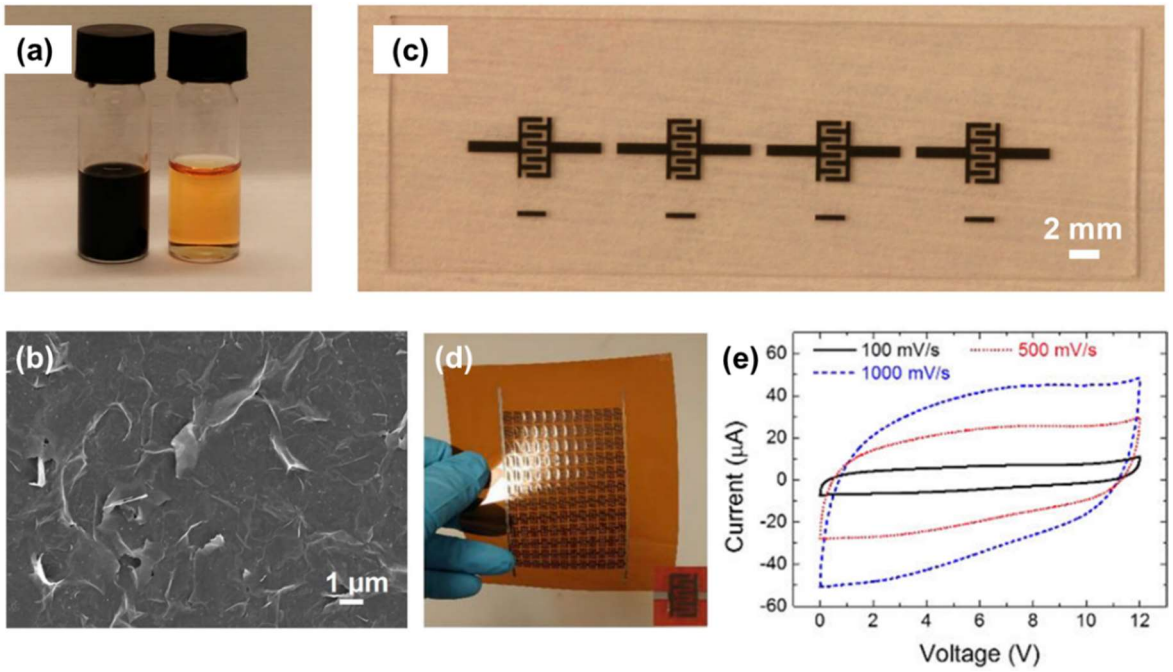

Fig. 5 Inkjet-printed MSCs using EG thin-film as microelectrodes. (a) Photographs of EG ink (black) and PSSH ink (orange) for printing the electrodes and electrolyte, respectively. (b) SEM image of the annealed EG electrode on a glass slide. (c) Photograph of four fully printed MSCs on a glass slide. (d) Photographs of a 12 in series × 12 in parallel MSC array on Kapton. (e) CV curves of the MSC array at different scan rates with a potential window of 12 V (The data was measured one month after the fabrication). Reproduced with permission.[153] Copyright 2017, American Chemical Society.

Si nanomembrane exhibited a highly wrinkled structure as shown in Fig. 4c. The wrinkles on the Si nanomembrane surface resulted from the huge volume change of the Si electrode during lithiation/delithiation. Generally, in bulk Si, the huge volume changes would lead to the pulverization of the electrodes because of strain-induced local deformation; in contrast, the Si nanomembrane electrode could accommodate large volume strains through forming a wrinkled structure, thus solving the poor cycle issues. In addition, at relatively low voltages, the currents through the Si nanomembrane gradually increased with the voltage changes (Fig. 4d and e), which could be attributed to the formation of conductive Li_xSi alloy. The increase and decrease of conductivity during lithiation/delithiation is suitable for real-time analysis of the electrochemical reaction in the microelectrode. Thus, such kind of MB provides a facile and direct way to monitor the electrochemical behavior of 2D materials.

2.2. MSCs

MSCs, as a new generation of microsized power source, have attracted considerable attention owing to their ultrahigh power densities, fast rate capabilities, and excellent cycle lifetimes.[66-68] Several studies have already reviewed fiber-shape MSCs;[45, 46, 69, 70] thus in this review we will only focus on in-plane and 3D MSCs. Unlike fiber-shape MSCs for wearable electronics,[71, 72] in-plane and 3D MSCs are usually designed for implantable and portable microdevices. Various 2D materials such as graphene, TMOs/TMHs, TMDs, MXenes, and 2D organic framework materials have been demonstrated to fabricate thin films or microelectrode finger arrays for MSCs.

On the other hand, the microfabrication technologies for microelectrodes of MSCs can be classified into two categories. The first category refers to the direct synthesis of electrode materials on the patterned current collectors. The related techniques including CVD,[73-75] laser scribing,[76-89] pyrolysis,[90-95] and electrolytic deposition[96-100] have been developed to realize MSCs. The second category involves indirect fabrication based on the existing electrode materials in powder or solution states. The microelectrode finger arrays can be constructed by inkjet printing,[101-113] spray coating,[74, 108, 114-119] drop and spin coating,[120-122] vacuum filtration,[123-125] LBL assembly,[126-131] and electrophoretic deposition.[132, 133] In this respect, the preparation of a stable dispersion with good solution processability is the vital concern. The advantages and disadvantages of the strategies mentioned above are detailed in Table 1.

2.2.1 Graphene

Graphene is the most extensively studied 2D material for MSCs owing to its unique 2D structural features associated with large specific surface area, high mechanical strength, chemical stability, and superior electrical conductivity.[11, 134] The theoretical capacitance of single-layer graphene was reported to be approximately 21 μF cm^{-2}.[135] In principle, a graphene-based SC could achieve a capacitance of approximately 550 F g^{-1} if its entire surface area could be fully exploited. Thus far, a variety of strategies, such as CVD growth,[74, 82] liquid-phase exfoliation,[101, 106, 107, 136, 137] electrochemical exfoliation,[108, 138-140] laser reduction,[83, 89, 141] chemical and thermal reduction,[77, 142-146] have been developed to fabricate graphene-based capacitive and Faradic film microelectrodes, as discussed below.

Table 1 Comparisons of the fabrication techniques for interdigital microelectrodes.

Techniques	Advantages	Disadvantages
Chemical vapor deposition	Controlled structure and design	Time-consuming, rigorous reaction conditions, high cost, low mass loading
Electrolytic deposition	Cost-effective, efficient, simple, eco-friendly, large-scale production	Uncontrolled growth in a lateral direction
Electrophoretic deposition	Simple, economic, controlled thickness	Limited by the charged species
Inkjet printing	Precise control, scalable, efficient, low-cost, commercially available	Complicated ink preparation, relatively low resolution
Drop coating	Time and energy saving	Heterogeneous, low production efficiency
Spin coating	Simple, large-scale fabrication, thickness control	Complicated preparation process for homogeneous solution
Spray coating	Effective, facile, simple	Relatively heterogeneous film
Vacuum filtration	Simple, low-cost, convenient, controllable thickness and construction	Size and shape limited by the used instrument
Layer-by-layer assembly	Economic, facile, robust	Complex preparation procedure
Laser scribing	Simple, scalable, cost-effective	Non-universal
Pyrolysis	One-step synthesis	High temperature, complex process
Painting	Versatile, simple, cost-effective	Low resolution

CVD-grown graphene for MSCs. CVD is an attractive method for fabricating high-quality graphene for microelectrodes. In 2014, Fischer *et al.*[73] reported the micrometers-thick graphitic petal microelectrodes by using microwave plasma CVD growth, optical lithography and reactive ion etching. After electrochemical oxidation treatment in an aqueous acidic solution, the enhancement of surface wettability with introduced oxygen-rich functional groups rendered easy accessibility of electrolyte ions to the microelectrodes. As a result, the fabricated MSCs exhibited an energy density of 9.5 mWh cm^{-3} at a scan rate of 20 mV s^{-1} and a power density of 235 W cm^{-3} at a scan rate of 50 V s^{-1}, much higher than those of MSCs without electrochemical treatment. Although the porous structure and great electrical conductivity of CVD-grown graphene microelectrodes resulted in high power density, the limited mass loading per unit area or volume was the limiting factor for the low energy density. In-situ growth or electrodeposition of high pseudocapacitive materials such as RuO_2, MnO_2, and polyaniline (PANI) on CVD-grown graphene microelectrodes may offer promising strategies to improve the energy densities.

Solution-processable high-quality graphene for MSCs. Liquid-phase exfoliation of graphite by ultrasonication is a promising strategy for the production of high-quality graphene due to its simplicity and scalability.[147, 148] The solution-processable graphene flakes can be used to fabricate microelectrode finger arrays by inkjet printing.[149] For example, in 2013, Li *et al.*[101] prepared stable high-concentration inks (1 mg mL^{-1}) with ultrasound-exfoliated graphene flakes for printing MSCs. Nonetheless, this exfoliation process required long-last agitation (40 h), delivering low exfoliation yields (~1%) and small sheet sizes (<1 μm). In the last few years, electrochemical exfoliation of graphite has emerged as an attractive method,[150-152] which produced electrochemically exfoliated graphene (EG) with large sheet size, large carbon to oxygen ratio and high electrical conductivity. In addition, EG can be processed into high-concentration graphene inks for printing MSCs. For example, in 2016, our group demonstrated directly printable in-plane MSCs using EG inks (0.8 mg mL^{-1}). The fabricated MSCs on paper substrates offered an areal capacitance as high as 5.4 mF cm^{-2}. Later in 2017, we reported the fabrication of EG inks with even higher concentration (2.3 mg mL^{-1}), containing ethyl cellulose as stabilizer and mixed solvent of cyclohexanone and terpineol.[153] Due to the high electrical conductivity, the printed EG could serve as both the electrodes and current collectors. More importantly, poly(4-styrenesulfonic acid) (PSSH) ink acting as a solid-state electrolyte was directly printed onto the surface of EG interdigital electrodes (Fig. 5a). The SEM image (Fig. 5b) manifested that the printed EG microelectrode patterns containing large graphene flakes were highly uniform. As displayed in Fig. 5c, the fabricated EG-based MSCs exhibited an areal capacitance of approximately 0.7 mF cm^{-2}. This simple fabrication process allowed for easy and efficient integration of the MSCs array in arbitrary connections to a large scale. For instance, large-scale MSC arrays consisting of more than 100 devices were manufactured on both rigid Si/SiO_2 wafer and flexible Kapton substrate (Fig. 5d). The cyclic voltammetry (CV) curves at different scan rates showed that the arrays could deliver 12 V at 1 V s^{-1} (Fig. 5e). Thus, the relatively mature printing technology and commercially available printers make inkjet printing promising for mass-produced MSCs for potential industrial scale.

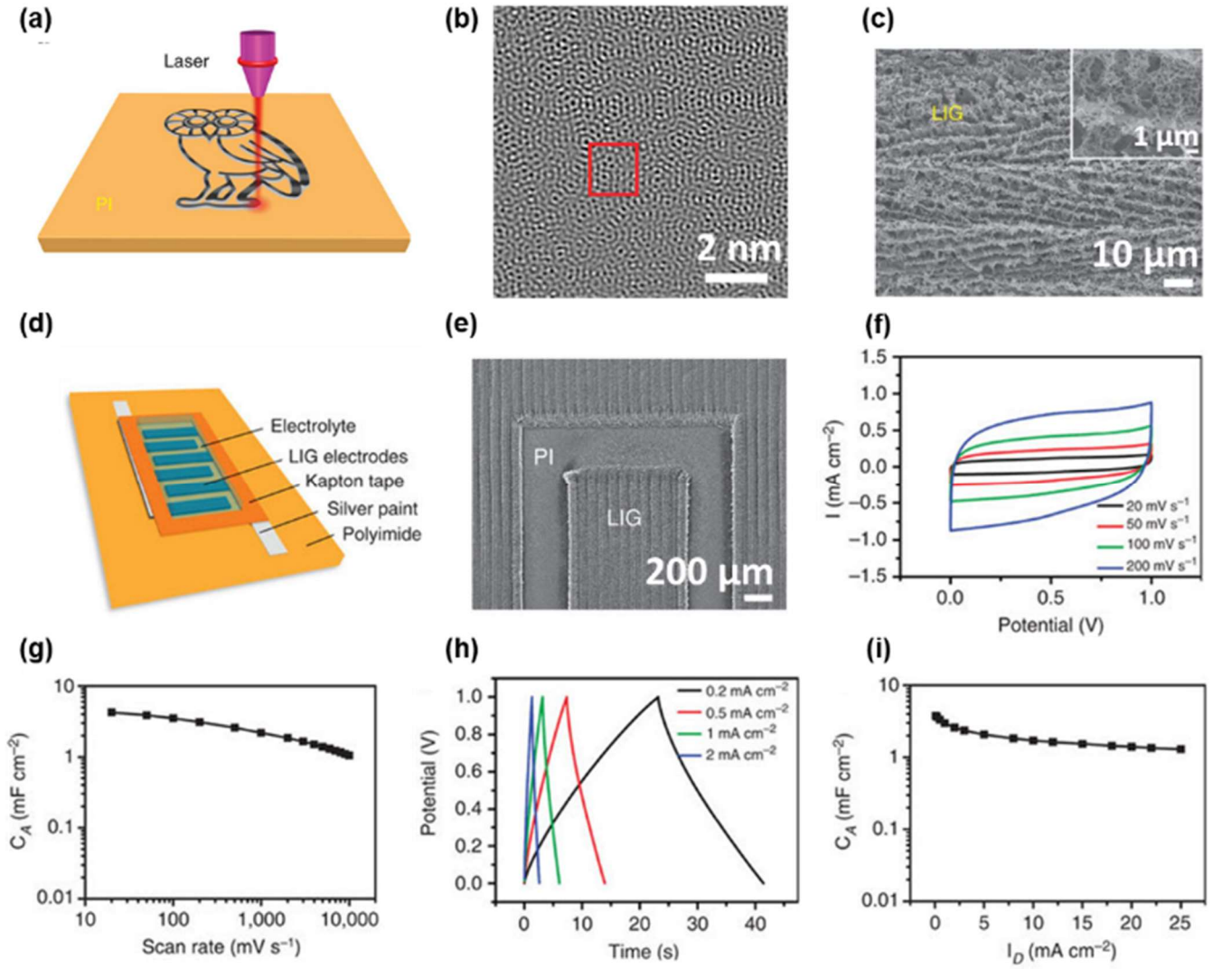

Fig. 6 LIG-based MSCs with porous graphene networks. (a) Schematic of the synthetic process of LIG from PI. (b) Cs-STEM image taken at the edge of a LIG flake. (c) SEM image of the LIG film. (d) Schematic of LIG-MSCs. (e) SEM image of LIG electrodes. (f) CV curves of LIG-MSCs at scan rates of 20-200 mV s^{-1}. (g) Areal capacitance calculated from CV curves as a function of scan rates. (h) GCD curves of LIG-MSCs at different current densities of 0.2-2 mA cm^{-2}. (i) Areal capacitance calculated from GCD curves. Reproduced with permission.[165] Copyright 2014, Macmillan Publishers Limited.

rGO for MSCs. Apart from high-quality graphene produced by CVD and exfoliation methods described above, rGO from reduction of GO has been applied in the fabrication of graphene microelectrodes.[154-161] In 2011, Ajayan *et al.*[141] firstly reduced and patterned hydrated GO films by laser irradiation. A porous morphology was formed due to the gas release from the decomposition of the functional groups and water upon localized laser heating. This was beneficial to ion accessibility during electrochemical measurements. Laser-scribing technique has advantages for fabricating MSCs due to its simple, scalable, clean, and cost-effective process. Similarly, later in 2012, Kaner *et al.* reported a standard LightScribe DVD optical drive for the direct laser reduction of GO to graphene.[83, 143, 162, 163] The prepared mechanically robust, highly electrical conductive rGO film with large specific surface area was extended for direct use in MSCs. More than 100 MSCs were produced on a single disc in 30 min or less. The rGO-based MSCs exhibited a power density of 200 W cm^{-3}, a frequency response of 19 ms, and a low leakage current. Afterwards, in order to improve the power density, our group demonstrated in 2013, graphene-based in-plane MSCs based on methane plasma reduced graphene (MPG) films micropatterned on both rigid and flexible substrates.[125] Due to the high electrical conductivity (345 S cm^{-1}) of the MPG interdigital electrode, the resultant MSCs delivered an areal capacitance of 80.7 μF cm^{-2} and a stack capacitance of 17.9 F cm^{-3} with PVA/H_2SO_4 gel electrolyte; moreover, these devices showed a volumetric power density of 495 W cm^{-3} and energy density of 2.5 mWh cm^{-3}.

Although the performance of rGO-based MSCs has been significantly improved by developing above scalable manufacturing technologies and designed architectures, their power and energy densities remained much lower than those of electrolytic capacitors and lithium thin-film batteries. Heteroatom doping in rGO could considerably enhance its capacitance through additional Faradaic reactions, also known as pseudocapacitance effects.[129, 164] In this respect, in 2014, our group reported a nitrogen and boron co-doped graphene film

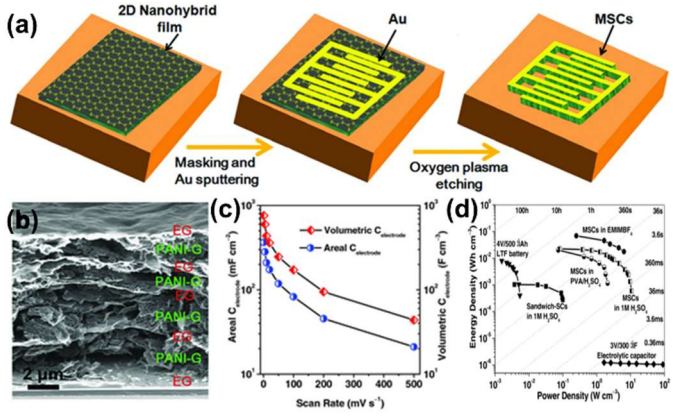

Fig. 7 In-plane MSCs based on the alternately stacked 2D structure with two PANI-G layers and three EG layers. (a) Schematic of fabrication of in-plane MSCs with interdigital electrodes. (b) Cross-sectional SEM image of a 2D nanohybrid film. (c) Areal and volumetric capacitances of P2G3-based MSC in PVA/H_2SO_4 gel electrolyte. (d) Ragone plots for P2G3-based MSCs in different electrolytes, sandwich SCs, Li thin-film battery (4 V/500 μAh), and electrolytic capacitor (3 V/300 μF). Reproduced with permission.[183] Copyright 2015, John Wiley & Sons, Inc.

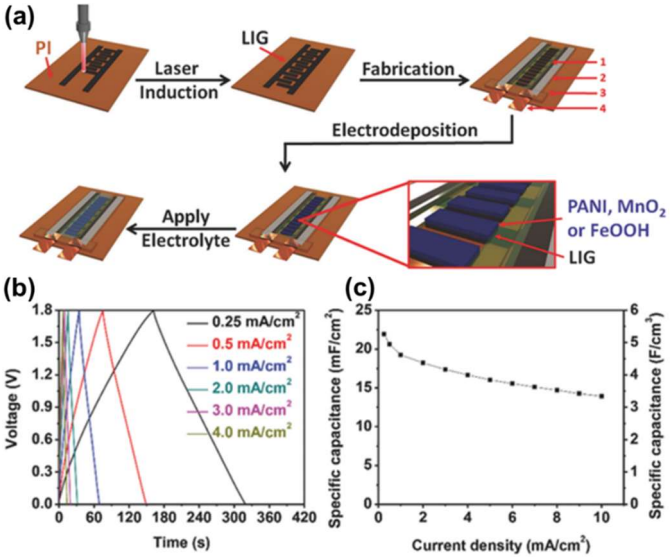

Fig. 8 In-plane LIG-FeOOH//LIG-MnO_2 AMSCs. (a) Scheme of the fabrication of MSCs with LIG-MnO_2, LIG-FeOOH, or LIG-PANI. (b) GCD curves of LIG-FeOOH//LIG-MnO_2 AMSCs at current densities ranging from 0.25 to 4.0 mA cm^{-2}. (c) Areal and volumetric capacitances of LIG-FeOOH//LIG-MnO_2 AMSCs at current densities of 0.25-10 mA cm^{-2}. Reproduced with permission.[209] Copyright 2016, John Wiley & Sons, Inc.

by the LBL assembly and thermal annealing treatment of hybrid film based on anionic GO nanosheets and cationic poly-L-Lysine.[129] The fabricated MSCs provided pronounced pseudocapacitive behavior with volumetric capacitance of 488 F cm^{-3}, higher than that of nitrogen-doped graphene (425 F cm^{-3}) and undoped rGO (245 F cm^{-3}).

Porous graphene for MSCs. The inevitable aggregation of graphene nanosheets severely reduces the available surface area and limits electron and ion transport in MSCs. Therefore, porous graphene is a fascinating material for MSCs. In 2014, Tour *et al.*[165, 166] demonstrated a scalable approach for producing and patterning porous graphene films directly from commercial polyimide film. Photothermal conversion of sp^3-carbon atoms to sp^2-carbon atoms was demonstrated by pulsed laser irradiation (Fig. 6a). As depicted in Fig. 6b, the aberration-corrected scanning transmission electron microscope (Cs-STEM) image showed the unusual ultra-polycrystalline feature of laser-induced graphene (LIG) flakes with disordered-grain boundaries. These defects could enhance electrochemical capacitance, as supported by theoretical calculations. SEM image of LIG film showed the porous foam structure resulting from the rapid liberation of gaseous products (Fig. 6c). The LIG prepared with a laser power of 5.4 W exhibited an electrical conductivity of ~25 S cm^{-1}, which was much higher than that of laser-reduced GO.[167] LIG-based in-plane MSCs delivered an areal capacitance of 4 mF cm^{-2} and a power density of approximately 9 mW cm^{-2} (Fig. 6d-i). However, the reported technique suffers from the limited compatibility with other substrates beyond polyimide.[168-170]

The aggregation of graphene could be also alleviated by hole structure[171-173] and nanochannel design.[174, 175] For instance, in 2015, Lee *et al.*[174] fabricated nanochanneled graphene film with the acid etchant for the removal of $Cu(OH)_2$ nanowires. The resultant hollow-graphene-based MSCs showed a volumetric capacitance of 368 F cm^{-3} at a current density of 0.3 A cm^{-3}, superior to that of the nonporous-graphene-based MSCs (98 F cm^{-3}), benefiting from efficient 2D ion transport pathways.

Graphene-based composites for MSCs. Graphene-based composites have been widely applied in MSCs with improved electrochemical performance due to the synergistic effects of graphene and other components.[176-182] For instance, in 2015, our group reported an alternately stacked PANI-graphene (PANI-G) and EG nanohybrid film as electrode materials for MSCs (Fig. 7a and b).[183] The optimal proportion of the alternately stacked structure was two PANI-G layers and three EG layers (denoted as P2G3). P2G3-based MSCs delivered areal and volumetric capacitances of 210 mF cm^{-2} and 436 F cm^{-3} at 10 mV s^{-1}, respectively (Fig. 7c and d). Such outstanding performance was attributed to the unique alternately stacked structure with a strong coupling effect between 2D pseudocapacitive PANI-G and capacitive EG nanosheets with accessible ion-transporting channels, an elastic spatial confinement effect, and a rapid electron transport pathway. In 2018, Fan *et al.* fabricated graphene-based mixed-dimensional hybrid aerogels (MDHA) for 3D-printing MSCs.[184] The hybrid ink with concentration up to 55 mg mL^{-1} was prepared by mixing MWCNTs, gluconic-*δ*-lactone and urea with GO dispersion. The 3D-printed interconnected hierarchical pores established unobstructed channels for ion transport in graphene/MWCNT MDHA. The achieved 3D MSCs delivered a maximum areal capacitance of 639 mF cm^{-2} at a current density of 4 mA cm^{-2} and sustained 90% capacitance after 10000 GCD cycles at 40 mA cm^{-2}.

2.2.2 TMOs/TMHs

Among various pseudocapacitive 2D materials, layered TMOs and TMHs have been widely studied due to their large theoretical capacities (typically 300–1,500 F g^{-1}), chemical

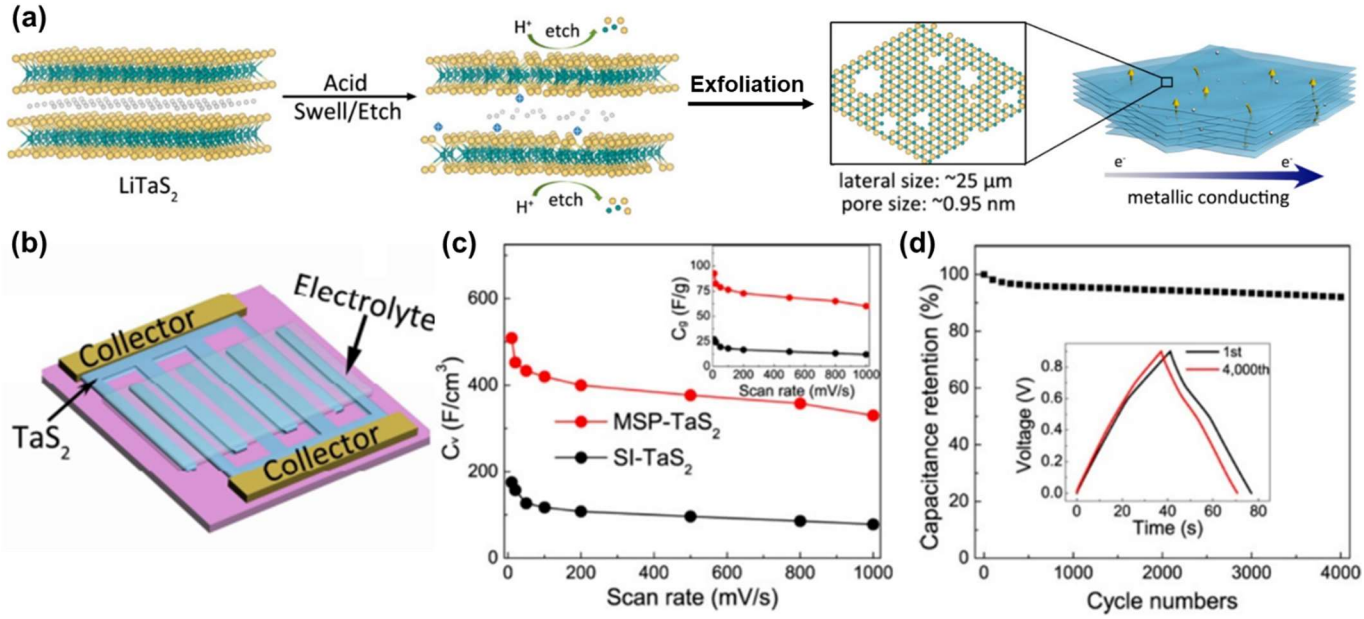

Fig. 9 In-plane MSCs based on exfoliated TaS_2 layers. (a) Schematic of the acid-assisted exfoliation method for TaS_2 monolayers. (b) Schematic of TaS_2-based MSCs. (c) Volumetric capacitance of MSP-TaS_2 and SI-TaS_2 based MSCs; inset shows the corresponding gravimetric capacitance as a function of scan rates. (d) Cycling stability of MSP-TaS_2 based MSC measured at 2 A g^{-1}; inset shows the comparison of GCD curves between the first cycle and the 4000th cycle. Reproduced with permission.[226] Copyright 2018, American Chemical Society.

stability and compatibility with electrolytes. They show multiple oxidation states, thus enabling rich redox reactions between electrodes and electrolyte ions.[185-190] As electrode materials for SCs, charge storage mainly arises from the pseudocapacitance caused by the fast redox reactions on their surfaces.[191-194] However, the poor electrical conductivity of layered TMOs/TMHs limits their coulombic efficiencies. For example, TMOs/TMHs usually possess low rate capability and poor cycling stability owing to the inherently poor electronic conductivity, slow reaction kinetics, and severe volume expansion during discharge/charge cycles. To overcome these obstacles, implanting defects/holes or vacancies, doping with other metallic elements and integrating with conductive matrix can be effective strategies. For instance, layered TMOs/TMHs such as MnO_2,[112, 185, 186, 191, 195-203] V_2O_5,[204] Bi_2O_3,[187] Co_3O_4,[189] $Co(OH)_2$,[205-207] $Ni(OH)_2$,[193, 208] FeOOH[209] have been composited with graphene, carbon nanotubes (CNTs), or metals, generating hybrid microelectrode materials for MSCs with enhanced performance. The status of performances of typical MSCs based on these materials is listed in Table 2.

Compared with symmetric MSCs using either EDLC or pseudocapacitive materials, asymmetric MSCs (AMSCs) in which positive and negative electrodes consisting of different active materials show superior overall performance.[196, 205, 210-217] Specifically, pseudocapacitive materials in one side of electrodes depend on a reversible redox reaction to serve as the energy source, whereas EDLC materials in another electrode store charge on the surface and supply high levels of power. The AMSCs with such design provide high capacitances and wide operation voltage windows of more than 1 V. For instance, in 2015, Kaner *et al.* demonstrated a 3D AMSC based on laser-scribed graphene-MnO_2 (LSG-MnO_2) as the positive electrode and LSG as the negative electrode using a laser-scribing technique and an electrodeposition method.[27] A charge balance between the two electrodes was obtained by precisely controlling the deposition time of MnO_2 nanosheets at the positive electrode and the thickness of the graphene film at the negative electrode. The achieved 3D AMSCs retained high rate capability with scan rates of up to 10000 mV s^{-1} and presented a wide potential window of 2.0 V in aqueous Na_2SO_4 electrolyte to afford a high volumetric energy density of 42 mWh cm^{-3}. The combination of such laser-induction technique and the electrodeposition method for AMSCs (Fig. 8a) was later employed in 2016 by Tour *et al*.[209] They electrodeposited three types of pseudocapacitive materials onto LIG, including MnO_2, FeOOH, and PANI. The areal and volumetric capacitances of LIG-FeOOH//LIG-MnO_2 AMSC reached 21.9 mF cm^{-2} and 5.4 F cm^{-3}, respectively, at a current density of 0.25 mA cm^{-2} with a potential window of 1.8 V (Fig. 8b and c). Moreover, the maximum areal and volumetric power densities were as high as 11853 μW cm^{-2} and 2891 mW cm^{-3}, respectively.

2.2.3 TMDs

Mono- and few-layer TMDs have attracted significant attention due to their tunable band gaps and vast natural reserves.[218-223] TMDs are a class of materials with the formula of MX_2, where M stands for a transition metal element from group IV to group VIII, and X is a chalcogen (S, Se, or Te).[224] Bulk TMDs have

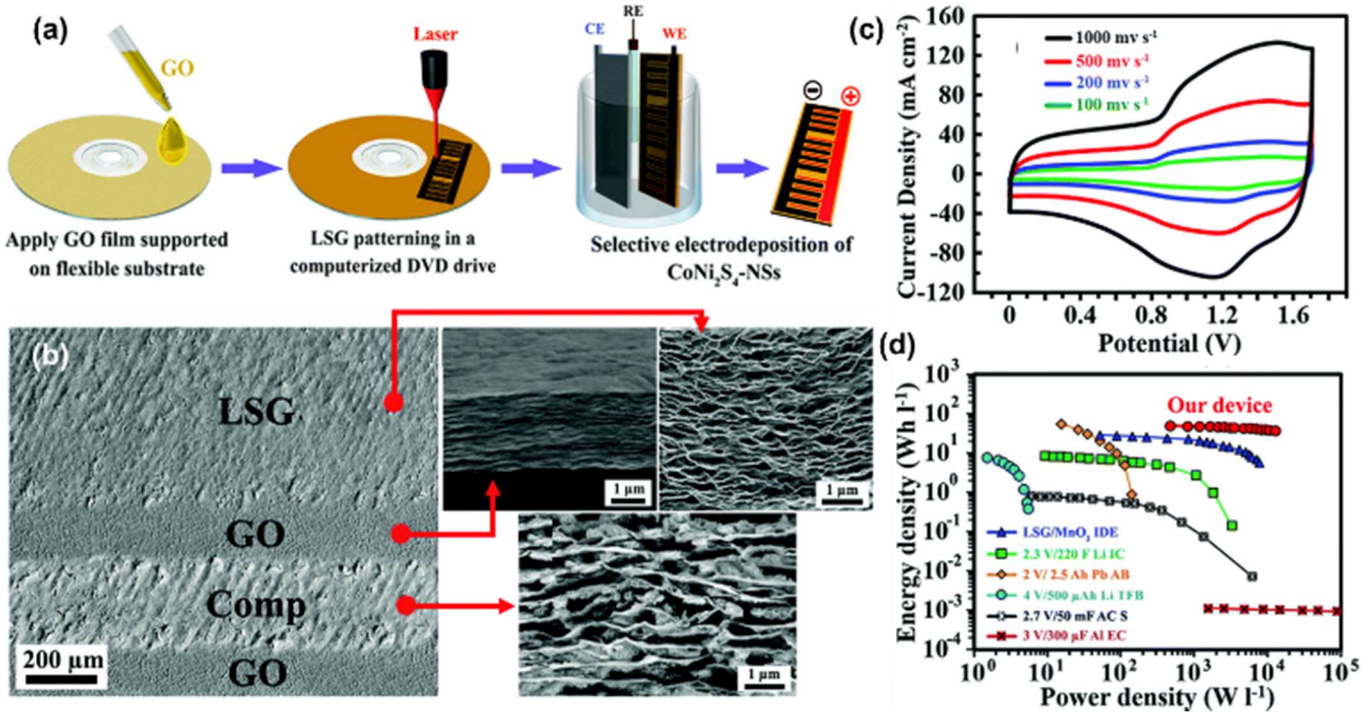

Fig. 10 In-plane hybrid MSCs with high operating voltage by laser scribing and electrodeposition. (a) Schematic of fabrication of LSG/$CoNi_2S_4$//LSG hybrid MSC. (b) SEM images of the as-prepared interdigital microelectrodes and corresponding cross-sectional SEM images of the GO, LSG and LSG/$CoNi_2S_4$ films. (c) CV curves at various scan rates. (d) Ragone plot of the LSG/$CoNi_2S_4$//LSG hybrid MSC compared with a number of commercially available energy storage devices. Reproduced with permission.[215] Copyright 2016, Royal Society of Chemistry.

diverse physical properties, including insulators such as HfS_2, semiconductors such as SnS_2 and MoS_2, semi-metals such as TiS_2 and WTe_2, and true metals such as TaS_2 and VSe_2. Metallic TMDs with high conductivities and large specific areas are favorable electrode materials for MSCs.[225, 226]

As one typical member of metallic TMDs, large-sized metallic sub-nanopore TaS_2 (MSP-TaS_2) was recently reported for MSCs by Xie *et al.*[226] Specifically, Fig. 9a showed the fabrication process of an acid-assisted exfoliation of single-crystalline TaS_2, achieving exfoliated metallic TaS_2 monolayer with tens of micrometers size and controllable in-plane sub-nanopores (0.95 nm). Hydrogen ion from the acid was utilized as an efficient and easily accessible assistant in simultaneous exfoliation and structural modification of TaS_2. The fast ion transport was achieved in TaS_2 monolayers due to their pore size matching well with that of electrolyte ion. MSP-TaS_2-based MSCs delivered a volumetric capacitance of 508 F cm^{-3} at a scan rate of 10 mV s^{-1}, which was about three times higher than that of small-sized (<1 µm) intact TaS_2-based MSCs (Fig. 9b and c). It could be explained by the fact that MSP-TaS_2 film had much higher electrical conductivity and appropriate-sized pores allowing Li^+ penetration from the surface throughout the whole framework. In addition, the MSP-TaS_2-based MSCs retained a capacitance in excess of 92% after 4000 cycles, indicating a good cycling stability (Fig. 9d).

Superior to above single-phase chalcogenides, the strongly coupled mixed-metal chalcogenides may synergistically enhance the electrochemical properties such as reversible capacity and electrical/ionic conductivity, which can yield improved electrochemical performance.[227] In 2016, Moosavifard *et al.* developed a facile, scalable and low cost process for fabricating LSG/$CoNi_2S_4$//LSG hybrid MSCs by combining direct laser reduction and selective electrodeposition (Fig. 10a).[215] Employing Faradaic LSG/$CoNi_2S_4$ as a positive electrode and EDLC LSG as a negative electrode in the hybrid MSC (Fig. 10b), the operating potential window could reach 1.7 V (Fig. 10c). Two pairs of redox peaks were attributable to the reversible Faradaic reactions of $Co^{2+}/Co^{3+}/Co^{4+}$ and Ni^{2+}/Ni^{3+} in alkaline PVA/KOH electrolyte. As shown in Fig. 10d, the LSG/$CoNi_2S_4$//LSG hybrid MSC delivered an excellent energy density up to 49 mWh cm^{-3}, and one individual device was able to power a red light-emitting diode (LED).

2.2.4 MXenes

MXenes ($M_{n+1}X_n$) are a class of emerging layered materials derived from $M_{n+1}AX_n$ precursors (M = Ti, V, Nb, *etc.*; A = Al, Si, Sn, *etc.*; n = 1, 2, or 3).[228-235] MAX phases show layered, hexagonal structures with M layers packed closely together in nearly hexagonal configurations. The A-element layers in MAX can be selectively etched by aqueous-fluoride-containing acidic solutions to obtain MXenes. Owing to the aqueous medium used during synthesis, MXene flakes are terminated with numerous surface functional groups containing O, OH, or F. MXenes exhibit good metallic conductivity and mechanical properties as well as hydrophilicity, making them good candidates for batteries and SCs.[236-246] The maximum theoretical capacity for MXenes was estimated to be ~615 C g^{-1}.[247]

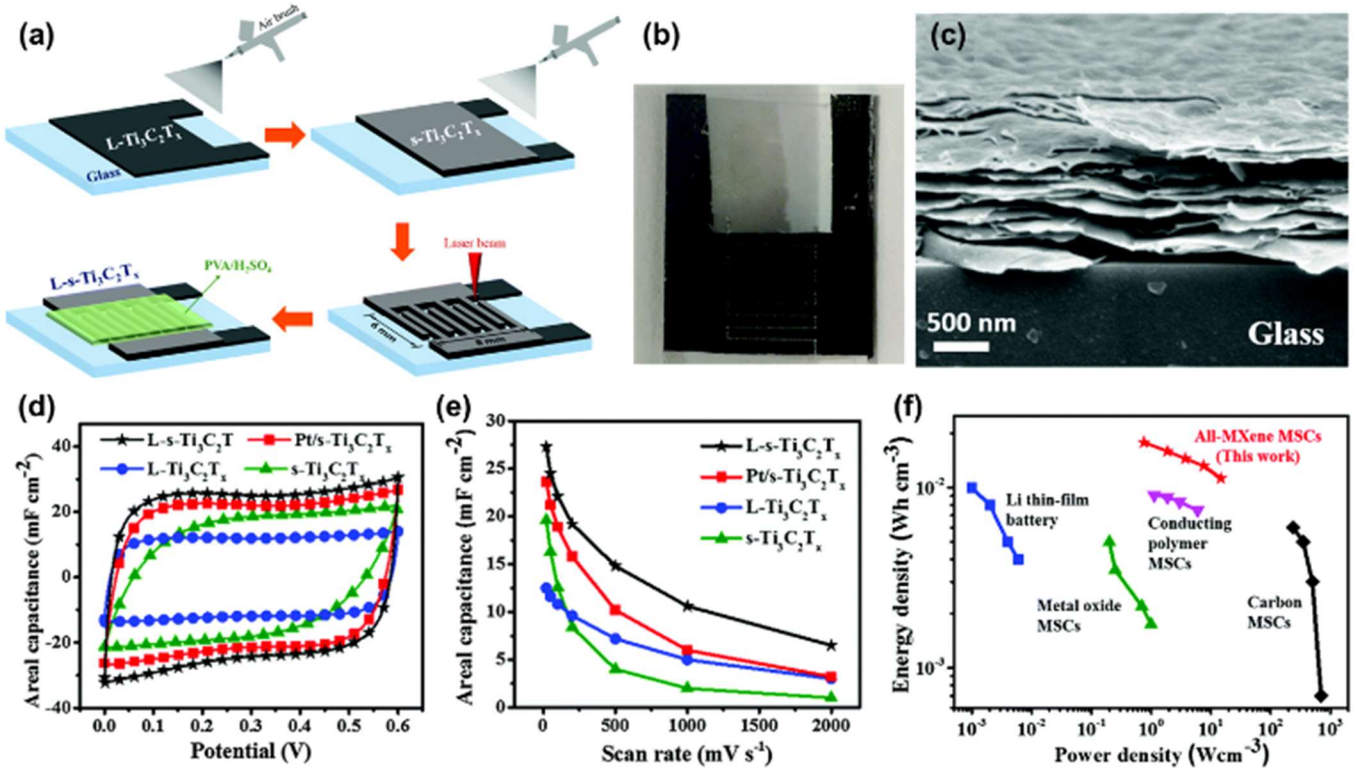

Fig. 11 Spray coating for all-MXene-based MSCs. (a) Schematic of fabrication process of all-$Ti_3C_2T_x$ MXene MSC. (b) Photograph of an interdigital L-s-$Ti_3C_2T_x$ MSC. (c) Cross-sectional SEM image of an L-s-$Ti_3C_2T_x$ MXene film. (d) CV curves at 50 mV s^{-1} and (e) areal capacitances with different scan rates of various MSCs. (f) Ragone plots for the all-MXene MSCs, Li thin-film batteries, and carbon, metal oxide, and conducting polymer-based MSCs. Reproduced with permission.[114] Copyright 2016, Royal Society of Chemistry.

In 2016, Gogotsi *et al.*[114] fabricated all solid-state MSCs with MXene serving as both the current collector (highly conductive, large-size (3–6 μm) $Ti_3C_2T_x$ (L-$Ti_3C_2T_x$) flakes) and active material (small-size (1 μm) $Ti_3C_2T_x$ (s-$Ti_3C_2T_x$) flakes) by a spray-coating method and direct laser cutting, as illustrated in Fig. 11a and b. The cross-sectional SEM image of the L-s-$Ti_3C_2T_x$ film demonstrated the restacking of the MXene flakes with good alignment, beneficial to the side-by-side ion/electron transport between microelectrodes (Fig. 11c). Compared with other types of MSCs based on $Ti_3C_2T_x$, L-s-$Ti_3C_2T_x$ MSC exhibited the best performance with an areal capacitance of 27.3 mF cm^{-2} and a volumetric capacitance of 356.8 F cm^{-3} (Fig. 11d-f). The MSC displayed excellent cycling stability without capacitance decay after 10000 cycles at 50 mV s^{-1}.

2.2.5 2D Organic framework materials

2D organic framework materials including 2D MOFs and 2D COFs are an emerging class of porous crystalline materials with designable periodical porous structure and tunable functionality.[248-250] The heteroatoms (B, N, O and S) on the precise locations of frameworks may exhibit redox activity for the pseudocapacitance. The high porosity from organic molecular assembly is beneficial to generate electrical double layer capacitance.[251, 252] Thus, 2D MOFs and COFs are regarded as potential electrode materials for electrochemical energy storage. However, the application of 2D organic framework materials in MSCs has been hindered by the lack of feasible microfabrication methods. In 2017, our group demonstrated a facile LBL method for fabricating on-chip MSCs based on an azulene-bridged coordination polymer framework (PiCBA) (Fig. 12).[253] Considering its rich aromatic skeleton, ultralow band gap, good carrier mobility, and permanent dipole moment of the azulene unit, PiCBA is a promising candidate for electrochemical energy storage. Therefore, PiCBA layers were directly grown onto the Au surface of the interdigital Au-SiO_2 substrate through the upright η^1 coordination of the terminal isocyanide carbon atoms and then integrated to fabricating MSCs using a PVA/H_2SO_4 gel electrolyte. The resultant MSCs delivered a specific capacitance of 34.1 F cm^{-3} at 50 mV s^{-1} and a volumetric power density of 1323 W cm^{-3}.

In general, apart from the above related fabrication methods demonstrated for various 2D active materials in MSCs, many other techniques such as painting,[254-256] filling,[257-260] and rolled-up technologies[261, 262] have been utilized to fabricate patterned electrode finger arrays or thin films. The realization of one MSC usually requires the combination of these different techniques. Table 2 summarizes fabricated in-plane and 3D MSCs based on 2D active materials reported in recent years.

3. Smart responsive MESDs

Along with the growing demand for intelligent electronic devices, extensive attentions have been paid to the smart or stimuli-responsive devices, which are responsive to the changes from either the external environment or devices themselves.[265-273] Recently, smart functions, including self-healing,[274, 275] electrochromism,[276, 277] shape memory,[278] photoluminescent,[279] photodetection,[280] and thermal

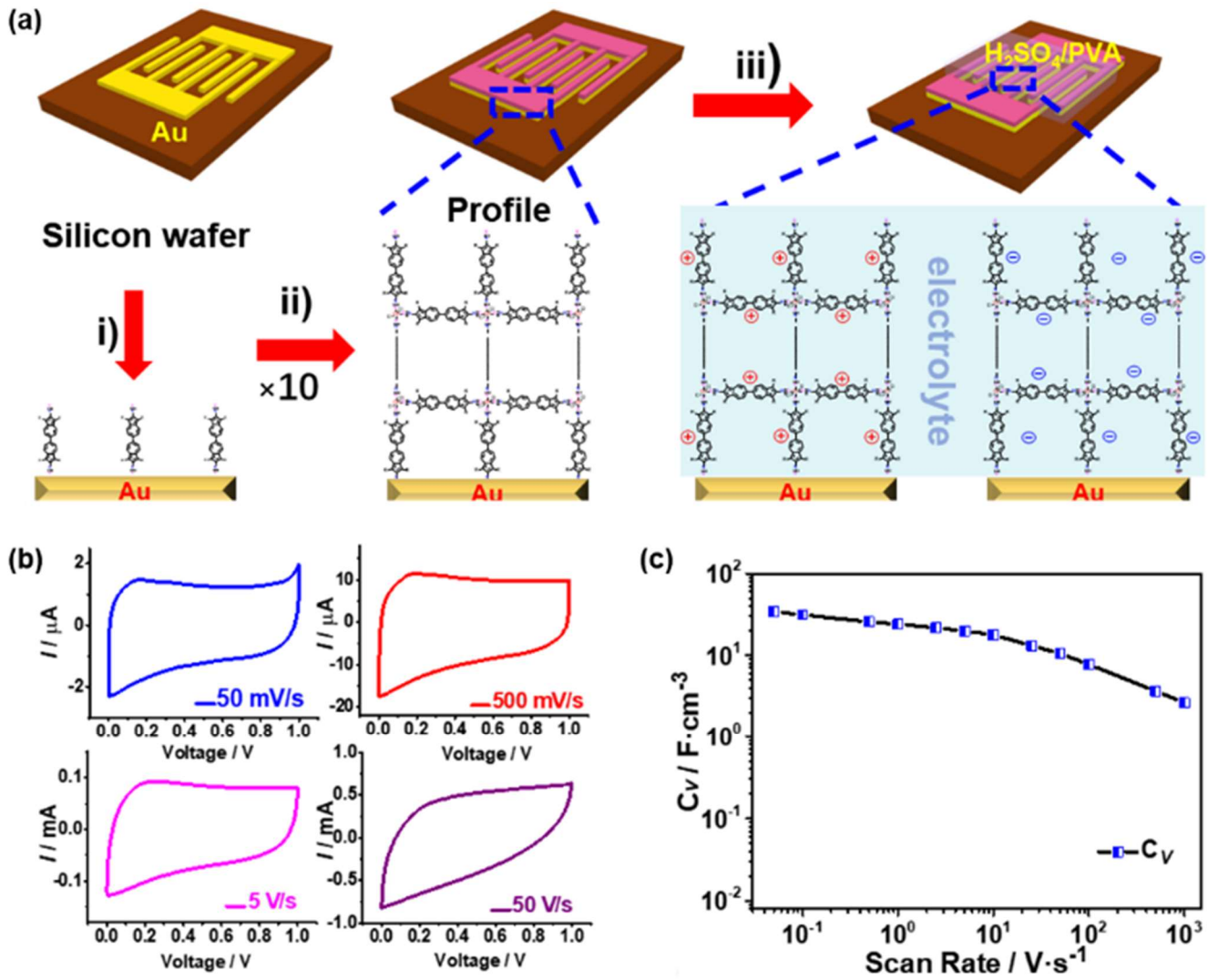

Fig. 12 LBL method for fabricating MSCs based on 2D conjugated polymer as microelectrodes. (a) Schematic of LBL fabrication of a PiCBA film on Au interdigital electrodes. (b) CV curves of PiCBA-based MSCs in PVA/H_2SO_4 gel electrolyte at different scan rates. (c) Volumetric capacitances of MSCs at different scan rates. Reproduced with permission.[253] Copyright 2017, John Wiley & Sons, Inc.

responsivity,[281-284] have been introduced into stimuli-responsive devices, which showed significant promise in the fields of healthcare, modern optoelectronics, biomimetic, artificial intelligence, and energy-related devices. However, the research and development of smart responsive MESDs are still at the early stage due to the poor compatibility among those stimuli, active materials, and processing technologies. Suitable materials, device designs, and appropriate performance levels are crucial for the practical applications of MESDs integrated with smart functions.

Currently, developments of functional electrolyte and functional electrode are two main strategies for introducing smart functions in MESDs. For example, in 2017, our group demonstrated the stimulus-responsive MSC (SR-MSC) with a reversible electrochromic window, as schematically illustrated in Fig. 13a.[285] By taking advantage of the synergistic effect of V_2O_5 nanoribbons and EG nanosheets, EG/V_2O_5 hybrid nanopaper was prepared as an electrode for MSCs, which provided a volumetric capacitance of 130.7 F cm^{-3} and a volumetric energy density of approximately 20 mWh cm^{-3} at 10 mV s^{-1}. Colorless viologen (MV^{2+}), a type of electrochromic molecule, could be reversibly reduced to the radical ion derivative of viologen (purple MV^{+}) upon accepting electrons (Fig. 13b). By using a PVA/LiCl gel electrolyte mixed with the methyl viologen, the resultant SR-MSCs exhibited a remarkable reversible electrochromic effect during the charge-discharge process within 0–1 V, providing a directly observable visual indication of their charge-discharge states (Fig. 13c and d). Very recently, we reported a novel thermoswitchable MSC with the self-protection function utilizing the thermodynamic behavior of a smart electrolyte, namely a lithium salt-dissolved polymer sol, poly(*N*-isopropylacrylamide)-*g*-methylcellulose.[284] Benefiting from the reversibility of ionic conductivity, the MSC exhibited a broad temperature window (30–80 °C) and totally switch-off behavior at 80 °C, as well as excellent cycling stability upon heating/cooling cycles. In the above two cases, the additive with smart function should be compatible with the chemical and physical properties of the electrolyte, without sacrificing the electrochemical performance of the MSCs.

Table 2 Summary of typical in-plane and 3D MSCs based on 2D active materials reported in recent years.

MSC (-)//(+)	Electrolyte	Voltage window / V	Specific capacitance		Device performance		Cycling stability	Ref.
			Areal / mF cm^{-2}	Volumetric / F cm^{-3}	Energy density	Power density		
EG//EG	PVA/H_2SO_4	0-1.0	5.4	27	-	-	5000 (90%)	108
rGO/rGO	PVA/H_2SO_4	0-0.8	17.9		2.5 mWh cm^{-3}	495 W cm^{-3}	10000 (98.3%)	125
LIG//LIG	1 M H_2SO_4	0-1.0	>4	1.5	-	9 mW cm^{-2}	9000 (100%)	165
LSG//LSG	PVA/H_2SO_4	0-1.0	2.32	3.05	-	200 W cm^{-3}	30000 (100%)	83
$Ti_3C_2T_x$//$Ti_3C_2T_x$	PVA/H_2SO_4	0-0.6	27	357	11-18 mWh cm^{-3}	0.7-15 W cm^{-3}	10000 (100%)	114
NPG/δ-MnO_2//NPG/δ-MnO_2	1 M Na_2SO_4	0-0.8	-	137	24.3 mWh cm^{-3}	295 W cm^{-3}	20000 (88%)	200
Ni@MnO_2//Ni@MnO_2	PVA/CH_3COOLi	0-0.8	52.9	-	11.1 mWh cm^{-3}	39.6 W cm^{-3}	5000 (80%)	199
Pt/Co_3O_4//Pt/Co_3O_4	1 M KOH	0-0.8	0.93	35.7	3.17 mWh cm^{-3}	47.4 W cm^{-3}	5000 (91.9%)	189
MnO_2/OLC//MnO_2/OLC	PVA/H_3PO_4	0-0.8	7.04	-	0.7 mWh cm^{-3}	80 mW cm^{-3}	1000 (80%)	112
SWCNT/carbon/MnO_2//SWCNT/carbon/MnO_2	PVA/H_3PO_4	0-0.8	0.55	20.4	-	-	5000 (92.4%)	191
Graphene-CNTCs//Graphene-CNTCs	1 M $BMIMBF_4$	0-3.0	3.93	1.96	2.42 mWh cm^{-3}	135 W cm^{-3}	8000 (98.4%)	263
rGO/Fe_2O_3//rGO/Fe_2O_3	PVA/KOH	0-1.0	0.34 7	11.57	1.61 mWh cm^{-3}	9.82 W cm^{-3}	32000 (92.08%)	142
rGO/$Co(OH)_2$//rGO/$Co(OH)_2$	1 M KOH	0-0.5	6	119	6 mWh cm^{-3}	390 mW cm^{-3}	5000 (77%)	205
MoS_2@rGO-MWCNT-carbon//MoS_2@rGO-MWCNT-carbon	PVA/H_2SO_4	0-1.0	13.7	-	1.9 μWh cm^{-2}	-	10000 (96.6%)	264
rGO-MnO_2-Ag NW//rGO-MnO_2-Ag NW	Fumed silica/BMIM TFSI	0-2.0	-	4.42	2.3 mWh cm^{-3}	162 mW cm^{-3}	6000 (90.3%)	144
Graphene-PANI//Graphene-PANI	PVA/H_2SO_4	0-1.0	210	436	11.7 mWh cm^{-3}	-	5000 (86.6%)	183
Fe_2O_3//MnO_2	1 M KOH	0-1.2	-	60	12 mWh cm^{-3}	14.8 W cm^{-3}	2500 (80%)	186
V_2O_5-PANI//MnO_2-PPy	5 M PVA/LiCl	0-1.6	-	-	15-20 mWh cm^{-3}	0.3-2.5 W cm^{-3}	7000 (92%)	204
NPG/MnO_2//NPG/PPy	PVA/LiCl	0-1.6	1.27	127	45.3 mWh cm^{-3}	440.4 W cm^{-3}	15000 (80%)	198
LIG-FeOOH//LIG-MnO_2	PVA/LiCl	0-1.8	21.9	5.4	2.4 mWh cm^{-3}	2891 mW cm^{-3}	2000 (84%)	209

LSG//LSG-MnO_2	1 M Na_2SO_4	0-2.0	400	250	22-42 mWh cm^{-3}	10 W cm^{-3}	10000 (96%)	27
CNF//$NiCo_2S_4$	1 M KOH	0-1.6	240 μAh cm^{-2}	-	200 μWh cm^{-2}	4.4 mW cm^{-2}	10000 (89%)	216
LSG//LSG-$CoNi_2S_4$	PVA/KOH	0-1.7	164	122.4	49 mWh cm^{-3}	13 W cm^{-3}	10000 (93.9%)	215

Apart from the electrolyte, designing functional electrode is another pathway to realize a smart response in MESDs. Surface functionalization of 2D electrode materials with functional molecules can be a straightforward method. In 2017, Müllen *et al.* demonstrated a photoswitchable MSC using a thin-film electrode based on diarylethene (DAE) adsorbed on the surface of graphene electrodes, thus creating a DAE-graphene (DAE-G) composite.[75] The efficient photo-isomerization behavior of DAE molecules was ascribed to reversible control of EDLC performance in the DAE-G composite. Photoswitching of the specific capacitance was enabled by the reversible control of interfacial charge injection into DAE molecular orbitals owing to charge transfer at the DAE-G interface upon light modulation. Nevertheless, the reversible ratio up to 20% was not high, possibly owing to the poor compatibility between graphene and DAE.

4. Smart integrated system

Although much progress has been made towards realizing high-performance MESDs in the past years as discussed above, much efforts remain needed for the practical applications of individual MESDs. Currently, most electronic devices are powered by bulky external power sources; externally connected power sources require space and energy. The recent boom in portable and implantable microelectronics has resulted in increasing requirements for self-powered systems. Thus, connecting individual MESD in series and parallel is a commonly used approach to achieve the required specific voltages and capacitances, which can be realized by rationally designing the structure of microelectrodes and the interconnections between them.[139] As the result, MESDs can be coupled with microsized

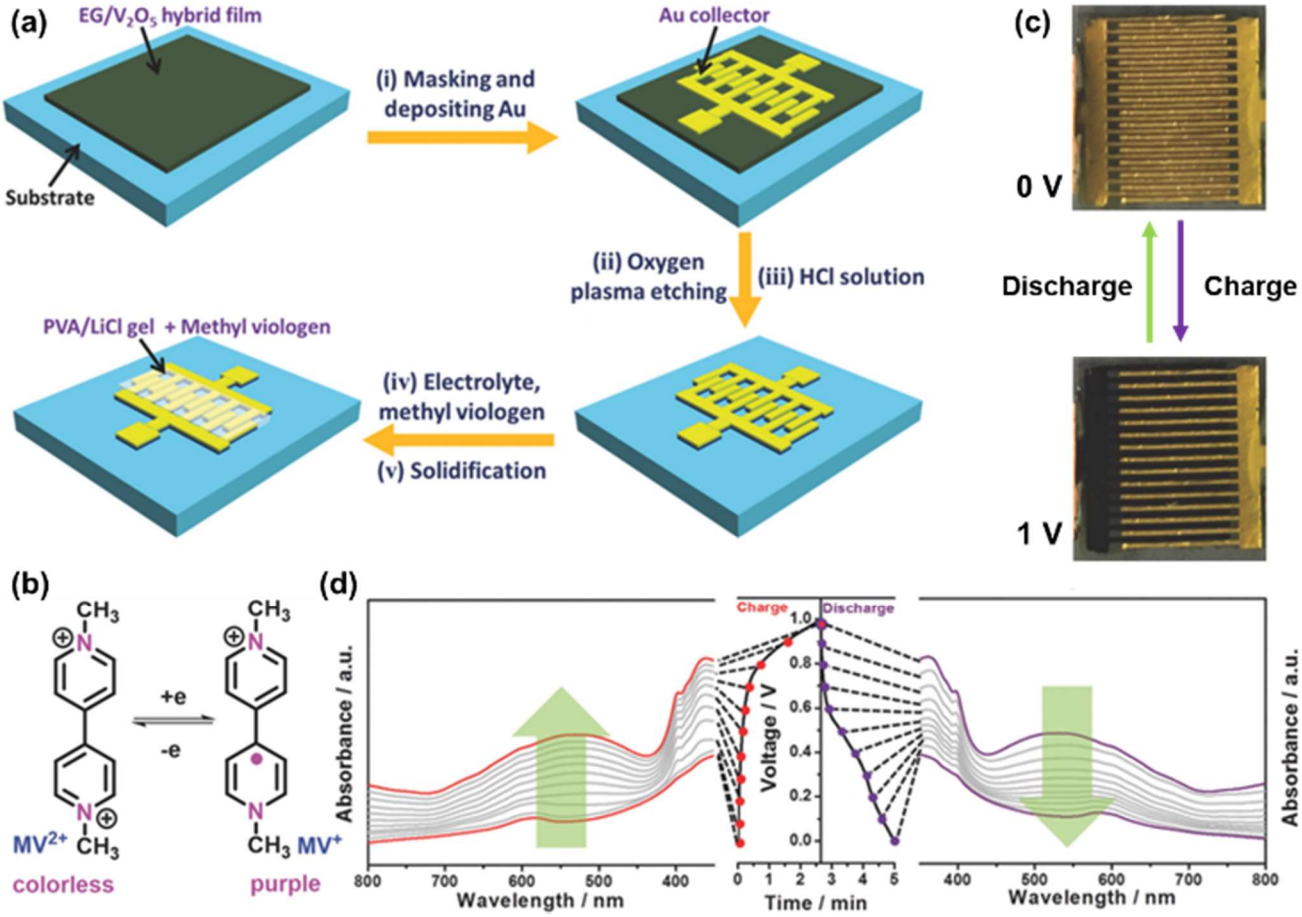

Fig. 13 Smart electrochromic MESD based on 2D EG/V_2O_5 microelectrodes. (a) Schematic fabrication of SR-MSCs. (b) Electrochromic mechanism of methyl viologen. (c) Photographs of reversible electrochromic effect of SR-MSCs during charge-discharge cycles. (d) UV-vis spectra of SR-MSCs at different voltages at a current density of 0.015 mA cm^{-2} between 0-1.0 V during one charge-discharge cycle. Reproduced with permission.[285] Copyright 2017, John Wiley & Sons, Inc.

energy harvesters to demonstrate high peak power, long lifetime, and high rate capability while maintaining reasonable energy densities for practical microelectronics.[286-289] Although some novel self-powered systems have been demonstrated,[290-292] the development of smart integrated system based on MESDs is still in its infancy.

MESDs/energy harvesting integrated systems. Numerous energy harvesting/conversion technologies including solar cells, piezoelectric generators, triboelectric generators, and thermoelectric generators have been developed in the past several decades, which can effectively convert renewable energy sources such as solar, mechanical, and thermal energy into electricity.[199, 293] Unsatisfactorily, a big shortcoming of these renewable sources is that electricity generation is highly dependent on their availability. In this regard, an effective strategy is to develop an integrated energy harvesting, conversion, and storage system that can simultaneously capture energy from the environment and store it by electrochemical energy storage devices.[294-296] Such intelligent integration is also applicable to miniaturized integrated energy systems.

Converting solar energy into electrical energy provides an attractive way to build energy-autonomous systems. In 2016, Watanabe *et al.* constructed a self-powered system by combining a commercial solar panel as the energy harvester, a LIG-based MSC as the energy storage unit and stabilizer, and a digital LCD clock as the working device, as illustrated in Fig. 14a.[76] The simultaneous function of the MSC as both energy storage unit and stabilizer was confirmed by recording the current and voltage changes of the different systems (Fig. 14b and c). These results clearly demonstrated the potential of such self-powered systems for wide-ranging applications in the future.

In addition to solar cell, various mechanical energies including wind, wave, and fluid motion can be also efficiently converted into electricity to power microdevices by using piezoelectric or triboelectric effects.[297-300] Among diverse nanogenerators, triboelectric nanogenerators (TENGs) have been extensively developed to extract almost all forms of ambient mechanical energies, especially human-motion-induced biomechanical energy, owing to the high output performance levels with their light weight.[170] For example, in 2018, Alshareef *et al.* reported a biocompatible self-charging power unit based on a TENG, a MXene-based MSC, and a rectifier.[299] It was sealed compactly by silicone rubber to harvest and store energy from human activities (Fig. 14d and e). The MXene-based MSC delivered a capacitance of 23 mF cm^{-2} with 95% capacitance retention up to 10000 charge-discharge cycles, while the TENG exhibited a maximum output power of 7.8 μW cm^{-2}. Fig. 14f illustrated the self-charging capability under hand clapping and the overall charging curve can be divided into 5 regions with alternative clapping and resting operations. It took about 30 min to charge the MSC to 0.6 V when continuously clapping without large current leakage.

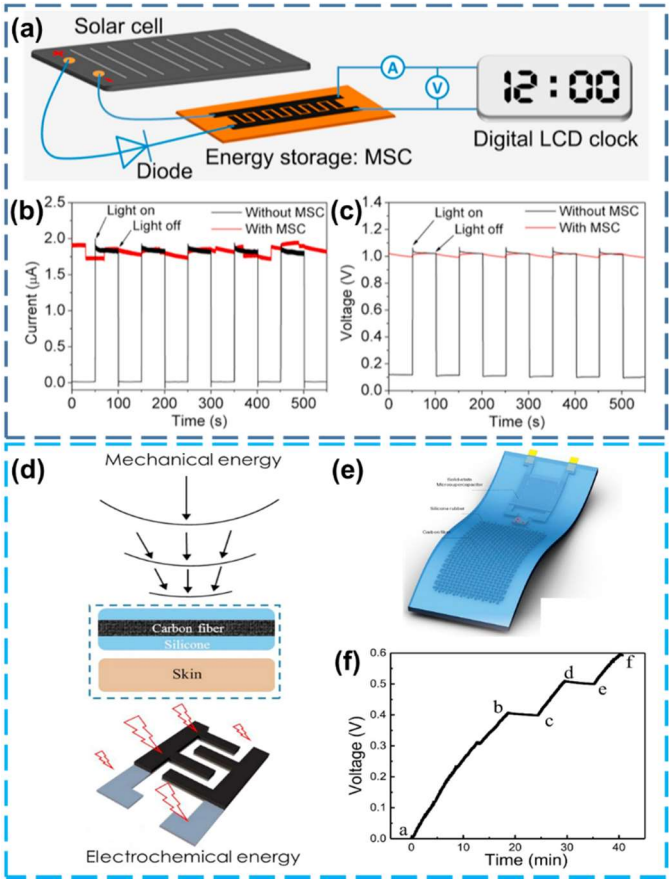

Fig. 14 Energy harvesting integrated systems. (a) Schematic of the circuit used for stabilization measurements combining a commercial solar cell (energy harvester), a diode, an MSC (energy storage and stabilizer), and a digital LCD clock (a working device). (b) Current and (c) voltage responses to the light illumination of the working circuit with and without an MSC by turning the light on/off. Reproduced with permission.[76] Copyright 2016, Elsevier. Schematic of (d) mechanism for generating electricity to charge the MSC and (e) the whole device. (f) Charging curve showing the voltage increase of the MSC powered by TENGs. Reproduced with permission.[299] Copyright 2018, Elsevier.

MESDs/sensing integrated systems. To acquire and transfer signals in sensing and communication procedures, self-powered sensors need power on the order of microwatts to milliwatts.[301-304] Adjustable power sources are essential for such low-energy applications. MESDs can offer enough power or voltage for such integrated systems. Self-powered photodetectors/sensors can be used for continuously and suitably monitoring personal healthcare and external environment without interruption.

UV photodetectors are able to convert UV light into electrical signals, which are important devices and used in various applications such as environmental monitoring, flame detection, and missile warning systems.[121, 305-307] Several self-powered UV photodetection systems have been recently fabricated by combining the MESDs with UV detectors.[76, 142, 204, 308, 309] As another increasingly common type of sensor, gas sensors have attracted increasing attention on environmental and safety monitoring. Integrating MESDs with a gas sensor makes the electronic device systems compact and lightweight, thus favoring their applications in portable and implantable electronics.[310-313] In 2017, Yan *et al.* reported an integrated device on one piece of paper.[313] AMSCs were integrated with a gas (NH_3 and HCl) sensor and charged by connecting it to a solar

cell. After being charged for 78 s, AMSCs achieved an open-circuit potential of 2.8 V and drove the gas sensor readily. The current alternately decreased and increased with the alternative introduction of NH_3 and HCl, proving the feasibility of this sustainably self-powered integrated device.

5. Summary and outlook

Emerging electrochemically active 2D materials open up a new window for the future development of high-performance, reliable and up-scalable MESDs. This review article has summarized recent achievements in versatile 2D materials, microfabrication methods and design techniques for MESDs. 2D materials, including graphene, TMOs/TMHs, TMDs, MXenes, and 2D organic framework materials have been studied in terms of their electrochemical properties for MSCs and MBs. On the other hand, device fabrication plays a key role in technology innovation that, in turn, influences the complexity and large-scale production of MESDs. It is also believed that introducing smart functions and integrating microdevices into systems are indispensable for promoting the robust growth of smart electronics. Considerable achievements in 2D materials based MESDs have been made in the fields of individual devices; and more recently, integrated systems based on such MESDs have been demonstrated which clearly highlight their potential application scopes. Nevertheless, some key technical challenges still need to be addressed. These include aspects such as individual device performance improvement, smart response design, and microdevice integration, as discussed below.

Aiming at the state-of-the-art MESD performance, structural engineering of 2D materials provides the solid foundation for tuning the chemical and physical properties including electrical conductivity, redox potential, crystal phase structure, and chemical stability. Approaches like heteroatom doping, defect/vacancy creation, surface/interface modification and heterostructure construction provide great opportunities for further improving the physicochemical properties of 2D materials. It is also well known that one big challenge faced by 2D materials lies in their inevitable aggregation due to their strong van-der-Waals interactions. To address this, one can enlarge the interlayer space toward improved storage capability or increased active sites by means of intercalation with guest molecules. Besides, for MESDs, vertically oriental 2D materials directly grown on interdigital current collectors is beneficial to achieving low interfacial resistance and facilitated charge transport. Moreover, in order to reach enhanced specific surface area and superior conductivity, combining different materials with 2D hybrids is a viable approach to overcome the limitations of each components. More importantly, the scalability and processability of high-quality 2D materials are essential not only for fundamental research, but also for the real industrial applications which require advanced microfabrication technologies including inkjet printing, 3D printing, and screen printing, *etc*.

In order to meet the demand for intelligent electronic devices, smart responsive MESDs have emerged as functional power sources. However, due to the miniaturized structure and complicated preparation process, only limited efforts have been devoted to developing MESDs with smart functions such as self-healing, compressibility, electrochromism, and stretchability. In this regard, it is important to use functional electrolytes or electrodes that are compatible with their working conditions and device structures. A variety of multi-responsive polymers like photosensitive, water-soluble, pH-sensitive, thermo-, electric-, and magnetic-responsive polymers can be further taken into consideration for the design of smart electrolytes. Furthermore, surface functionalization of 2D active materials sheds a light into the smart electrodes, due to the flexibility of tuning the electrical conductivity, surface area, as well as ion transport within the electrolyte. Therefore, the exploration of smart materials is equally important to the development of microfabrication technologies for MESDs.

As micropower sources and energy storage microdevices, MESDs based on 2D materials are ultimately aimed at powering ready-to-use energy-consuming microelectronics. Owing to the complicated fabrication process of smart integrated systems, only few works have been demonstrated so far. Thus, innovative self-powered integrated systems involving energy harvesting, energy storage, and energy consumption units represents a highly attractive research direction. In addition, the design of smart integrated system with foldable, washable, and biodegradable features can pave the way for future intelligent, independent and continuous operation of daily electronics. At last, these all-in-one self-powered systems could be highly expected to benefit healthcare applications in the future.

Abbreviations

2D	Two-dimensional
3D	Three-dimensional
AMSCs	Asymmetric microsupercapacitors
$BMIMBF_4$	1-butyl-3-methylimidazolium tetrafluoroborate
BMIM TFSI	1-butyl-3-methylimidazolium bis(trifluoromethylsulfonyl)imide
CNFs	Carbon nanofibers
CNTs	Carbon nanotubes
CNTCs	Carbon nanotube carpets
CV	Cyclic voltammetry
CVD	Chemical vapor deposition
DAE	Diarylethene
DFT	Density functional theory
EDLCs	Electric double-layer capacitors
EG	Electrochemically exfoliated graphene
GCD	Galvanostatic charge/discharge
GO	Graphene oxide
LBL	Layer-by-layer
LED	Light-emitting diode
LIG	Laser-induced graphene
LSG	Laser-scribed graphene
MBs	Microbatteries
MESDs	Miniaturized energy storage devices
MSCs	Microsupercapacitors

MV	Methyl viologen
MWCNTs	Multi-walled carbon nanotubes
MXenes	Transition metal carbides/nitrides
NPG	Nanoporous gold
NPs	Nanoparticles
NWs	Nanowires
OLC	Onion-like carbon
PANI	Polyaniline
PPy	Polypyrrole
PSC	Perovskite solar cell
PSSH	Poly(4-styrenesulfonic acid)
PVA	Polyvinyl alcohol
rGO	Reduced graphene oxide
SCs	Supercapacitors
SEM	Scanning electron microscope
SWCNTs	Single-wall carbon nanotubes
TEM	Transmission electron microscope
TENGs	Triboelectric nanogenerators
TMDs	Transition metal dichalcogenides
TMHs	Transition metal hydroxides
TMOs	Transition metal oxides

Conflicts of interest

The authors declare no competing financial interest.

Acknowledgements

This work is supported by the German Research Foundation (DFG) within the Cluster of Excellence 'Center for Advancing Electronics Dresden' (cfaed) and financed by the Initiative and Networking Fund of the German Helmholtz Association, Helmholtz International Research School for Nanoelectronic Networks NanoNet (VH-KO-606), Hamburg Science Award, ERC Grant on 2DMATER, HIPER-G, and EU Graphene Flagship.

References

1 B. Dunn, H. Kamath and J.-M. Tarascon, *Science*, 2011, **334**, 928-935.
2 M. R. Lukatskaya, B. Dunn and Y. Gogotsi, *Nat. Commun.*, 2016, **7**, 12647.
3 M. F. El-Kady, Y. Shao and R. B. Kaner, *Nat. Rev. Mater.*, 2016, **1**, 16033.
4 C. Liu, F. Li, L.-P. Ma and H.-M. Cheng, *Adv. Mater.*, 2010, **22**, E28-E62.
5 P. Simon, Y. Gogotsi and B. Dunn, *Science*, 2014, **343**, 1210-1211.
6 P. G. Bruce, S. A. Freunberger, L. J. Hardwick and J.-M. Tarascon, *Nat. Mater.*, 2012, **11**, 19-29.
7 N. A. Kyeremateng, T. Brousse and D. Pech, *Nat. Nanotechnol.*, 2017, **12**, 7-15.
8 S. Ferrari, M. Loveridge, S. D. Beattie, M. Jahn, R. J. Dashwood and R. Bhagat, *J. Power Sources*, 2015, **286**, 25-46.
9 J. C. Ruiz-Morales, A. Tarancon, J. Canales-Vazquez, J. Mendez-Ramos, L. Hernandez-Afonso, P. Acosta-Mora, J. R. Marin Rueda and R. Fernandez-Gonzalez, *Energy Environ. Sci.*, 2017, **10**, 846-859.
10 J. Liu, J. Wang, C. Xu, H. Jiang, C. Li, L. Zhang, J. Lin and Z. X. Shen, *Adv. Sci.*, 2017, DOI: 10.1002/advs.201700322, 1700322.
11 F. Bonaccorso, L. Colombo, G. Yu, M. Stoller, V. Tozzini, A. C. Ferrari, R. S. Ruoff and V. Pellegrini, *Science*, 2015, **347**, 1246501.
12 D. P. Dubal, O. Ayyad, V. Ruiz and P. Gomez-Romero, *Chem. Soc. Rev.*, 2015, **44**, 1777-1790.
13 G. Wang, L. Zhang and J. Zhang, *Chem. Soc. Rev.*, 2012, **41**, 797-828.
14 P. Simon and Y. Gogotsi, *Nat. Mater.*, 2008, **7**, 845-854.
15 Y. Gogotsi and P. Simon, *Science*, 2011, **334**, 917-918.
16 X. Wang, Y. Chen, O. G. Schmidt and C. Yan, *Chem. Soc. Rev.*, 2016, **45**, 1308-1330.
17 Z.-S. Wu, X. Feng and H.-M. Cheng, *Natl. Sci. Rev.*, 2014, **1**, 277-292.
18 A. S. Arico, P. Bruce, B. Scrosati, J.-M. Tarascon and W. van Schalkwijk, *Nat. Mater.*, 2005, **4**, 366-377.
19 Y.-Z. Zhang, Y. Wang, T. Cheng, W.-Y. Lai, H. Pang and W. Huang, *Chem. Soc. Rev.*, 2015, **44**, 5181-5199.
20 X. Lu, M. Yu, G. Wang, Y. Tong and Y. Li, *Energy Environ. Sci.*, 2014, **7**, 2160-2181.
21 J. Jiang, Y. Li, J. Liu, X. Huang, C. Yuan and X. W. Lou, *Adv. Mater.*, 2012, **24**, 5166-5180.
22 F. Wang, X. Wu, C. Li, Y. Zhu, L. Fu, Y. Wu and X. Liu, *Energy Environ. Sci.*, 2016, **9**, 3570-3611.
23 J. W. Choi and D. Aurbach, *Nat. Rev. Mater.*, 2016, **1**, 16013.
24 A. Tyagi, K. M. Tripathi and R. K. Gupta, *J. Mater. Chem. A*, 2015, **3**, 22507-22541.
25 L. Li, Z. Wu, S. Yuan and X.-B. Zhang, *Energy Environ. Sci.*, 2014, **7**, 2101-2122.
26 D. Yu, K. Goh, H. Wang, L. Wei, W. Jiang, Q. Zhang, L. Dai and Y. Chen, *Nat. Nanotechnol.*, 2014, **9**, 555-562.
27 M. F. El-Kady, M. Ihns, M. Li, J. Y. Hwang, M. F. Mousavi, L. Chaney, A. T. Lech and R. B. Kaner, *Proc. Natl. Acad. Sci. USA*, 2015, **112**, 4233-4238.
28 H. Hu, Z. Pei and C. Ye, *Energy Storage Mater.*, 2015, **1**, 82-102.
29 P. Huang, C. Lethien, S. Pinaud, K. Brousse, R. Laloo, V. Turq, M. Respaud, A. Demortière, B. Daffos, P. L. Taberna, B. Chaudret, Y. Gogotsi and P. Simon, *Science*, 2016, **351**, 691-695.
30 H. Ning, J. H. Pikul, R. Zhang, X. Li, S. Xu, J. Wang, J. A. Rogers, W. P. King and P. V. Braun, *Proc. Natl. Acad. Sci. USA*, 2015, **112**, 6573-6578.
31 K. Sun, T.-S. Wei, B. Y. Ahn, J. Y. Seo, S. J. Dillon and J. A. Lewis, *Adv. Mater.*, 2013, **25**, 4539-4543.
32 J. H. Pikul, H. Gang Zhang, J. Cho, P. V. Braun and W. P. King, *Nat. Commun.*, 2013, **4**, 1732.
33 K. Fu, Y. Wang, C. Yan, Y. Yao, Y. Chen, J. Dai, S. Lacey, Y. Wang, J. Wan, T. Li, Z. Wang, Y. Xu and L. Hu, *Adv. Mater.*, 2016, **28**, 2587-2594.
34 G. Xiong, C. Meng, R. G. Reifenberger, P. P. Irazoqui and T. S. Fisher, *Electroanalysis*, 2014, **26**, 30-51.
35 Y. Guo, Y. Wei, H. Li and T. Zhai, *Small*, 2017, **13**, 1701649.
36 K. S. Novoselov, A. K. Geim, S. V. Morozov, D. Jiang, Y. Zhang, S. V. Dubonos, I. V. Grigorieva and A. A. Firsov, *Science*, 2004, **306**, 666-669.
37 X. Y. Zhang, L. L. Hou, A. Ciesielski and P. Samori, *Adv. Energy Mater.*, 2016, **6**, 1600671.
38 Y. H. Xue, Q. Zhang, W. J. Wang, H. Cao, Q. H. Yang and L. Fu, *Adv. Energy Mater.*, 2017, **7**, 1602684.
39 Z. Wu, L. Li, J.-m. Yan and X.-b. Zhang, *Adv. Sci.*, 2017, **4**, 1600382.
40 B. Mendoza-Sanchez and Y. Gogotsi, *Adv. Mater.*, 2016, **28**, 6104-6135.
41 P. Y. Chen, M. Liu, Z. Wang, R. H. Hurt and I. Y. Wong, *Adv. Mater.*, 2017, **29**, 1605096.

42 Y. Zhu, L. Peng, Z. Fang, C. Yan, X. Zhang and G. Yu, *Adv. Mater.*, 2018, **30**, e1706347.
43 K.-S. Chen, I. Balla, N. S. Luu and M. C. Hersam, *ACS Energy Lett.*, 2017, **2**, 2026-2034.
44 K. S. Kumar, N. Choudhary, Y. Jung and J. Thomas, *ACS Energy Lett.*, 2018, **3**, 482-495.
45 X. Wang, K. Jiang and G. Shen, *Mater. Today*, 2015, **18**, 265-272.
46 D. Yu, Q. Qian, L. Wei, W. Jiang, K. Goh, J. Wei, J. Zhang and Y. Chen, *Chem. Soc. Rev.*, 2015, **44**, 647-662.
47 M. Beidaghi and Y. Gogotsi, *Energy Environ. Sci.*, 2014, **7**, 867-884.
48 J. F. M. Oudenhoven, L. Baggetto and P. H. L. Notten, *Adv. Energy Mater.*, 2011, **1**, 10-33.
49 P. V. Braun and R. G. Nuzzo, *Nat. Nanotechnol.*, 2014, **9**, 962.
50 J. Ni and L. Li, *Adv. Funct. Mater.*, 2018, **28**, 1704880.
51 Y. Wang, B. Liu, Q. Li, S. Cartmell, S. Ferrara, Z. D. Deng and J. Xiao, *J. Power Sources*, 2015, **286**, 330-345.
52 S. Liu, F. Wang, R. Dong, T. Zhang, J. Zhang, X. Zhuang, Y. Mai and X. Feng, *Adv. Mater.*, 2016, **28**, 8365-8370.
53 F. Wang, S. Xiao, M. Li, X. Wang, Y. Zhu, Y. Wu, A. Shirakawa and J. Peng, *J. Power Sources*, 2015, **287**, 416-421.
54 W. Faxing, L. Yu, W. Xiaowei, C. Zheng, W. Yuping and H. Rudolf, *ChemElectroChem*, 2015, **2**, 1024-1030.
55 M. L. Aubrey and J. R. Long, *J. Am. Chem. Soc.*, 2015, **137**, 13594-13602.
56 L. Xue, S. V. Savilov, V. V. Lunin and H. Xia, *Adv. Funct. Mater.*, 2018, **28**, 1705836.
57 C. Zhang, S.-H. Park, S. E. O'Brien, A. Seral-Ascaso, M. Liang, D. Hanlon, D. Krishnan, A. Crossley, N. McEvoy, J. N. Coleman and V. Nicolosi, *Nano Energy*, 2017, **39**, 151-161.
58 F. Wang, Z. Liu, P. Zhang, H. Li, W. Sheng, T. Zhang, R. Jordan, Y. Wu, X. Zhuang and X. Feng, *Small*, 2017, **13**, 1702449.
59 F. Yu, Z. Liu, R. Zhou, D. Tan, H. Wang and F. Wang, *Mater. Horiz.*, 2018, **5**, 529-535.
60 A. C. Serino, J. S. Ko, M. T. Yeung, J. J. Schwartz, C. B. Kang, S. H. Tolbert, R. B. Kaner, B. S. Dunn and P. S. Weiss, *ACS Nano*, 2017, **11**, 7995-8001.
61 J. Wang, J. Huang, R. Yan, F. Wang, W. Cheng, Q. Guo and J. Wang, *J. Mater. Chem. A*, 2015, **3**, 3144-3150.
62 G. Wang, J. Zhang, S. Yang, F. Wang, X. Zhuang, K. Müllen and X. Feng, *Adv. Energy Mater.*, 2017, DOI: 10.1002/aenm.201702254, 1702254.
63 W. Tian, S. Zhang, C. Huo, D. Zhu, Q. Li, L. Wang, X. Ren, L. Xie, S. Guo, P. K. Chu, H. Zeng and K. Huo, *ACS Nano*, 2018, **12**, 1887-1893.
64 J. He, C. Zhang, H. Du, S. Zhang, P. Hu, Z. Zhang, Y. Ma, C. Huang and G. Cui, *Electrochim. Acta*, 2015, **178**, 476-483.
65 W. Si, I. Mönch, C. Yan, J. Deng, S. Li, G. Lin, L. Han, Y. Mei and O. G. Schmidt, *Adv. Mater.*, 2014, **26**, 7973-7978.
66 D. Qi, Y. Liu, Z. Liu, L. Zhang and X. Chen, *Adv. Mater.*, 2016, **29**, 1602802.
67 N. Liu and Y. Gao, *Small*, 2017, **13**, 1701989.
68 F. Wang, X. Wu, X. Yuan, Z. Liu, Y. Zhang, L. Fu, Y. Zhu, Q. Zhou, Y. Wu and W. Huang, *Chem. Soc. Rev.*, 2017, **46**, 6816-6854.
69 X. Cai, M. Peng, X. Yu, Y. Fu and D. Zou, *J. Mater. Chem. C*, 2014, **2**, 1184-1200.
70 K. Jost, G. Dion and Y. Gogotsi, *J. Mater. Chem. A*, 2014, **2**, 10776-10787.
71 H. Sun, Y. Zhang, J. Zhang, X. Sun and H. Peng, *Nat. Rev. Mater.*, 2017, **2**, 17023.
72 W. Zeng, L. Shu, Q. Li, S. Chen, F. Wang and X.-M. Tao, *Adv. Mater.*, 2014, **26**, 5310-5336.
73 G. Xiong, C. Meng, R. G. Reifenberger, P. P. Irazoqui and T. S. Fisher, *Energy Technol.*, 2014, **2**, 897-905.
74 J. Yun, D. Kim, G. Lee and J. S. Ha, *Carbon*, 2014, **79**, 156-164.
75 Z. Liu, H. I. Wang, A. Narita, Q. Chen, Z. Mics, D. Turchinovich, M. Klaui, M. Bonn and K. Müllen, *J. Am. Chem. Soc.*, 2017, **139**, 9443-9446.
76 J. Cai, C. Lv and A. Watanabe, *Nano Energy*, 2016, **30**, 790-800.
77 J. Cai, C. Lv and A. Watanabe, *J. Mater. Chem. A*, 2016, **4**, 1671-1679.
78 H.-C. Huang, C.-J. Chung, C.-T. Hsieh, P.-L. Kuo and H. Teng, *Nano Energy*, 2016, **21**, 90-105.
79 J. B. In, B. Hsia, J.-H. Yoo, S. Hyun, C. Carraro, R. Maboudian and C. P. Grigoropoulos, *Carbon*, 2015, **83**, 144-151.
80 F. Wen, C. Hao, J. Xiang, L. Wang, H. Hou, Z. Su, W. Hu and Z. Liu, *Carbon*, 2014, **75**, 236-243.
81 B. Xie, Y. Wang, W. Lai, W. Lin, Z. Lin, Z. Zhang, P. Zou, Y. Xu, S. Zhou, C. Yang, F. Kang and C.-P. Wong, *Nano Energy*, 2016, **26**, 276-285.
82 L. Zhang, D. DeArmond, N. T. Alvarez, R. Malik, N. Oslin, C. McConnell, P. K. Adusei, Y.-Y. Hsieh and V. Shanov, *Small*, 2017, **13**, 1603114.
83 M. F. El-Kady and R. B. Kaner, *Nat. Commun.*, 2013, **4**, 1475.
84 Z. Peng, R. Ye, J. A. Mann, D. Zakhidov, Y. Li, P. R. Smalley, J. Lin and J. M. Tour, *ACS Nano*, 2015, **9**, 5868-5875.
85 P. Yadav, A. Basu, A. Suryawanshi, O. Game and S. Ogale, *Adv. Mater. Interfaces*, 2016, **3**, 1600057.
86 L. V. Thekkekara, B. Jia, Y. Zhang, L. Qiu, D. Li and M. Gu, *Appl. Phys. Lett.*, 2015, **107**, 031105.
87 R. Kumar, E. Joanni, R. K. Singh, E. da Silva, R. Savu, L. T. Kubota and S. A. Moshkalev, *J. Colloid Interface Sci.*, 2017, **507**, 271-278.
88 X. Yun, Z. Xiong, L. Tu, L. Bai and X. Wang, *Carbon*, 2017, **125**, 308-317.
89 R. P. R.-Z. Li, K. D. Kihm, S. Bai, D. Bridges, U. Tumuluri, Z. Wu, and G. C. T. Zhang, Z. Feng, A. Hu, *Energy Environ. Sci.*, 2016, **9**, 1458-1467.
90 B. Hsia, M. S. Kim, M. Vincent, C. Carraro and R. Maboudian, *Carbon*, 2013, **57**, 395-400.
91 C. Shen, X. Wang, W. Zhang and F. Kang, *Sci. Rep.*, 2013, **3**, 2294.
92 S. Wang, B. Hsia, C. Carraro and R. Maboudian, *J. Mater. Chem. A*, 2014, **2**, 7997-8002.
93 L. Wei, N. Nitta and G. Yushin, *ACS Nano*, 2013, **7**, 6498-6506.
94 M. Beidaghi, W. Chen and C. Wang, *J. Power Sources*, 2011, **196**, 2403-2409.
95 Y. Yang, L. He, C. Tang, P. Hu, X. Hong, M. Yan, Y. Dong, X. Tian, Q. Wei and L. Mai, *Nano Res.*, 2016, **9**, 2510-2519.
96 A. Ferris, S. Garbarino, D. Guay and D. Pech, *Adv. Mater.*, 2015, **27**, 6625-6629.
97 T. M. Dinh, A. Achour, S. Vizireanu, G. Dinescu, L. Nistor, K. Armstrong, D. Guay and D. Pech, *Nano Energy*, 2014, **10**, 288-294.
98 N. Kurra, M. K. Hota and H. N. Alshareef, *Nano Energy*, 2015, **13**, 500-508.
99 H. Hu, K. Zhang, S. Li, S. Ji and C. Ye, *J. Mater. Chem. A*, 2014, **2**, 20916-20922.
100 K. Wang, W. Zou, B. Quan, A. Yu, H. Wu, P. Jiang and Z. Wei, *Adv. Energy Mater.*, 2011, **1**, 1068-1072.
101 J. Li, F. Ye, S. Vaziri, M. Muhammed, M. C. Lemme and M. Östling, *Adv. Mater.*, 2013, **25**, 3985-3992.
102 K.-H. Choi, J. Yoo, C. K. Lee and S.-Y. Lee, *Energy Environ. Sci.*, 2016, **9**, 2812-2821.
103 W. Liu, C. Lu, H. Li, R. Y. Tay, L. Sun, X. Wang, W. L. Chow, X. Wang, B. K. Tay, Z. Chen, J. Yan, K. Feng, G. Lui, R. Tjandra, L. Rasenthiram, G. Chiu and A. Yu, *J. Mater. Chem. A*, 2016, **4**, 3754-3764.
104 S. Wang, N. Liu, J. Tao, C. Yang, W. Liu, Y. Shi, Y. Wang, J. Su, L. Li and Y. Gao, *J. Mater. Chem. A*, 2015, **3**, 2407-2413.

105 Y. Xiao, L. Huang, Q. Zhang, S. Xu, Q. Chen and W. Shi, *Appl. Phys. Lett.*, 2015, **107**, 013906.
106 W. J. Hyun, E. B. Secor, C.-H. Kim, M. C. Hersam, L. F. Francis and C. D. Frisbie, *Adv. Energy Mater.*, 2017, **7**, 1700285.
107 L. Li, E. B. Secor, K.-S. Chen, J. Zhu, X. Liu, T. Z. Gao, J.-W. T. Seo, Y. Zhao and M. C. Hersam, *Adv. Energy Mater.*, 2016, **6**, 1600909.
108 Z. Liu, Z.-S. Wu, S. Yang, R. Dong, X. Feng and K. Müllen, *Adv. Mater.*, 2016, **28**, 2217-2222.
109 D. Pech, M. Brunet, P.-L. Taberna, P. Simon, N. Fabre, F. Mesnilgrente, V. Conédéra and H. Durou, *J. Power Sources*, 2010, **195**, 1266-1269.
110 H. Su, P. Zhu, L. Zhang, F. Zhou, X. liang, T. Li, Q. Wang, R. Sun and C. Wong, *Sustainable Energy Fuels*, 2017, **1**, 1601-1610.
111 H. Pang, Y. Zhang, W.-Y. Lai, Z. Hu and W. Huang, *Nano Energy*, 2015, **15**, 303-312.
112 Y. Wang, Y. Shi, C. X. Zhao, J. I. Wong, X. W. Sun and H. Y. Yang, *Nanotechnology*, 2014, **25**, 094010.
113 Y. Wang, Y.-Z. Zhang, D. Dubbink and J. E. ten Elshof, *Nano Energy*, 2018, **49**, 481-488.
114 Y.-Y. Peng, B. Akuzum, N. Kurra, M.-Q. Zhao, M. Alhabeb, B. Anasori, E. C. Kumbur, H. N. Alshareef, M.-D. Ger and Y. Gogotsi, *Energy Environ. Sci.*, 2016, **9**, 2847-2854.
115 J. Pu, X. Wang, R. Xu and K. Komvopoulos, *ACS Nano*, 2016, **10**, 9306-9315.
116 D. Kim, G. Lee, D. Kim and J. S. Ha, *ACS Appl. Mater. Interfaces*, 2015, **7**, 4608-4615.
117 S. Wang, Z.-S. Wu, S. Zheng, F. Zhou, C. Sun, H.-M. Cheng and X. Bao, *ACS Nano*, 2017, **11**, 4283-4291.
118 D. Kim, G. Shin, Y. J. Kang, W. Kim and J. S. Ha, *ACS Nano*, 2013, **7**, 7975-7982.
119 H. Kim, J. Yoon, G. Lee, S.-h. Paik, G. Choi, D. Kim, B.-M. Kim, G. Zi and J. S. Ha, *ACS Appl. Mater. Interfaces*, 2016, **8**, 16016-16025.
120 B. Song, L. Li, Z. Lin, Z.-K. Wu, K.-s. Moon and C.-P. Wong, *Nano Energy*, 2015, **16**, 470-478.
121 J. Xu and G. Shen, *Nano Energy*, 2015, **13**, 131-139.
122 Z.-S. Wu, Y.-Z. Tan, S. Zheng, S. Wang, K. Parvez, J. Qin, X. Shi, C. Sun, X. Bao, X. Feng and K. Müllen, *J. Am. Chem. Soc.*, 2017, **139**, 4506-4512.
123 H. Xiao, Z.-S. Wu, F. Zhou, S. Zheng, D. Sui, Y. Chen and X. Bao, *Energy Storage Mater.*, 2018, **13**, 233-240.
124 S. Wang, Z.-S. Wu, F. Zhou, X. Shi, S. Zheng, J. Qin, H. Xiao, C. Sun and X. Bao, *npj 2D Materials and Applications*, 2018, **2**, 7.
125 Z. S. Wu, K. Parvez, X. Feng and K. Müllen, *Nat. Commun.*, 2013, **4**, 2487.
126 G. Lee, D. Kim, J. Yun, Y. Ko, J. Cho and J. S. Ha, *Nanoscale*, 2014, **6**, 9655-9664.
127 G. Lee, D. Kim, D. Kim, S. Oh, J. Yun, J. Kim, S.-S. Lee and J. S. Ha, *Energy Environ. Sci.*, 2015, **8**, 1764-1774.
128 Y. Lim, J. Yoon, J. Yun, D. Kim, S. Y. Hong, S.-J. Lee, G. Zi and J. S. Ha, *ACS Nano*, 2014, **8**, 11639-11650.
129 Z.-S. Wu, K. Parvez, A. Winter, H. Vieker, X. Liu, S. Han, A. Turchanin, X. Feng and K. Müllen, *Adv. Mater.*, 2014, **26**, 4552-4558.
130 Z.-K. Wu, Z. Lin, L. Li, B. Song, K.-s. Moon, S.-L. Bai and C.-P. Wong, *Nano Energy*, 2014, **10**, 222-228.
131 S. Y. Hong, J. Yoon, S. W. Jin, Y. Lim, S.-J. Lee, G. Zi and J. S. Ha, *ACS Nano*, 2014, **8**, 8844-8855.
132 D. Pech, M. Brunet, H. Durou, P. Huang, V. Mochalin, Y. Gogotsi, P.-L. Taberna and P. Simon, *Nat. Nanotechnol.*, 2010, **5**, 651-654.
133 P. Huang, D. Pech, R. Lin, J. K. McDonough, M. Brunet, P.-L. Taberna, Y. Gogotsi and P. Simon, *Electrochem. Commun.*, 2013, **36**, 53-56.
134 X. Wang, X. Lu, B. Liu, D. Chen, Y. Tong and G. Shen, *Adv. Mater.*, 2014, **26**, 4763-4782.
135 J. Xia, F. Chen, J. Li and N. Tao, *Nat. Nanotechnol.*, 2009, **4**, 505-509.
136 J. Li, V. Mishukova and M. Östling, *Appl. Phys. Lett.*, 2016, **109**, 123901.
137 S. Sollami Delekta, A. D. Smith, J. Li and M. Ostling, *Nanoscale*, 2017, **9**, 6998-7005.
138 H. Xiao, Z.-S. Wu, L. Chen, F. Zhou, S. Zheng, W. Ren, H.-M. Cheng and X. Bao, *ACS Nano*, 2017, **11**, 7284-7292.
139 X. Shi, Z. S. Wu, J. Qin, S. Zheng, S. Wang, F. Zhou, C. Sun and X. Bao, *Adv. Mater.*, 2017, **29**, 1703034.
140 Z.-S. Wu, Y. Zheng, S. Zheng, S. Wang, C. Sun, K. Parvez, T. Ikeda, X. Bao, K. Müllen and X. Feng, *Adv. Mater.*, 2017, **29**, 1602960.
141 W. Gao, N. Singh, L. Song, Z. Liu, A. L. M. Reddy, L. Ci, R. Vajtai, Q. Zhang, B. Wei and P. M. Ajayan, *Nat. Nanotechnol.*, 2011, **6**, 496-500.
142 S. Gu, Z. Lou, L. Li, Z. Chen, X. Ma and G. Shen, *Nano Res.*, 2015, **9**, 424-434.
143 Y. Shao, J. Li, Y. Li, H. Wang, Q. Zhang and R. B. Kaner, *Mater. Horiz.*, 2017, **4**, 1145-1150.
144 W. Liu, C. Lu, X. Wang, R. Y. Tay and B. K. Tay, *ACS Nano*, 2015, **9**, 1528-1542.
145 S. Byun and J. Yu, *J. Power Sources*, 2016, **307**, 849-855.
146 J. Qin, F. Zhou, H. Xiao, R. Ren and Z.-S. Wu, *Sci. China Mater.*, 2017, **26**, 949-965.
147 J. N. Coleman, M. Lotya, A. O'Neill, S. D. Bergin, P. J. King, U. Khan, K. Young, A. Gaucher, S. De, R. J. Smith, I. V. Shvets, S. K. Arora, G. Stanton, H.-Y. Kim, K. Lee, G. T. Kim, G. S. Duesberg, T. Hallam, J. J. Boland, J. J. Wang, J. F. Donegan, J. C. Grunlan, G. Moriarty, A. Shmeliov, R. J. Nicholls, J. M. Perkins, E. M. Grieveson, K. Theuwissen, D. W. McComb, P. D. Nellist and V. Nicolosi, *Science*, 2011, **331**, 568-571.
148 V. Nicolosi, M. Chhowalla, M. G. Kanatzidis, M. S. Strano and J. N. Coleman, *Science*, 2013, **340**, 1226419.
149 G. Hu, J. Kang, L. W. T. Ng, X. Zhu, R. C. T. Howe, C. G. Jones, M. C. Hersam and T. Hasan, *Chem. Soc. Rev.*, 2018, **47**, 3265-3300.
150 S. Yang, M. R. Lohe, K. Müllen and X. Feng, *Adv. Mater.*, 2016, **28**, 6213-6221.
151 S. Yang, S. Brüller, Z.-S. Wu, Z. Liu, K. Parvez, R. Dong, F. Richard, P. Samorì, X. Feng and K. Müllen, *J. Am. Chem. Soc.*, 2015, **137**, 13927-13932.
152 S. Yang, A. G. Ricciardulli, S. Liu, R. Dong, M. R. Lohe, A. Becker, M. A. Squillaci, P. Samorì, K. Müllen and X. Feng, *Angew. Chem. Int. Ed.*, 2017, **56**, 6669-6675.
153 J. Li, S. Sollami Delekta, P. Zhang, S. Yang, M. R. Lohe, X. Zhuang, X. Feng and M. Östling, *ACS Nano*, 2017, **11**, 8249-8256.
154 Z. Pei, H. Hu, G. Liang and C. Ye, *Nano-Micro Lett.*, 2016, **9**, 19.
155 G. Sun, J. An, C. K. Chua, H. Pang, J. Zhang and P. Chen, *Electrochem. Commun.*, 2015, **51**, 33-36.
156 K. Shen, J. Ding and S. Yang, *Adv. Energy Mater.*, 2018, **0**, 1800408.
157 L. Peng, X. Peng, B. Liu, C. Wu, Y. Xie and G. Yu, *Nano Lett.*, 2013, **13**, 2151-2157.
158 M. Xue, F. Li, J. Zhu, H. Song, M. Zhang and T. Cao, *Adv. Funct. Mater.*, 2012, **22**, 1284-1290.
159 Y. Wang, W. Lai, N. Wang, Z. Jiang, X. Wang, P. Zou, Z. Lin, H. J. Fan, F. Kang, C.-P. Wong and C. Yang, *Energy Environ. Sci.*, 2017, **10**, 941-949.
160 X. Wang, F. Wan, L. Zhang, Z. Zhao, Z. Niu and J. Chen, *Adv. Funct. Mater.*, 2018, **0**, 1707247.
161 Z. Niu, L. Zhang, L. Liu, B. Zhu, H. Dong and X. Chen, *Adv. Mater.*, 2013, **25**, 4035-4042.

162 M. F. El-Kady, V. Strong, S. Dubin and R. B. Kaner, *Science*, 2012, **335**, 1326-1330.
163 J. Y. Hwang, M. F. El-Kady, Y. Wang, L. Wang, Y. Shao, K. Marsh, J. M. Ko and R. B. Kaner, *Nano Energy*, 2015, **18**, 57-70.
164 Z.-S. Wu, A. Winter, L. Chen, Y. Sun, A. Turchanin, X. Feng and K. Müllen, *Adv. Mater.*, 2012, **24**, 5130-5135.
165 J. Lin, Z. Peng, Y. Liu, F. Ruiz-Zepeda, R. Ye, E. L. Samuel, M. J. Yacaman, B. I. Yakobson and J. M. Tour, *Nat. Commun.*, 2014, **5**, 5714.
166 Y. Li, D. X. Luong, J. Zhang, Y. R. Tarkunde, C. Kittrell, F. Sargunaraj, Y. Ji, C. J. Arnusch and J. M. Tour, *Adv. Mater.*, 2017, **29**, 1700496.
167 V. Strong, S. Dubin, M. F. El-Kady, A. Lech, Y. Wang, B. H. Weiller and R. B. Kaner, *ACS Nano*, 2012, **6**, 1395-1403.
168 A. Basu, K. Roy, N. Sharma, S. Nandi, R. Vaidhyanathan, S. Rane, C. Rode and S. Ogale, *ACS Appl. Mater. Interfaces*, 2016, **8**, 31841-31848.
169 J. Lee, J. Y. Seok, S. Son, M. Yang and B. Kang, *J. Mater. Chem. A*, 2017, **5**, 24585-24593.
170 J. Luo, F. R. Fan, T. Jiang, Z. Wang, W. Tang, C. Zhang, M. Liu, G. Cao and Z. L. Wang, *Nano Res.*, 2015, **8**, 3934-3943.
171 H. Sun, L. Mei, J. Liang, Z. Zhao, C. Lee, H. Fei, M. Ding, J. Lau, M. Li, C. Wang, X. Xu, G. Hao, B. Papandrea, I. Shakir, B. Dunn, Y. Huang and X. Duan, *Science*, 2017, **356**, 599-604.
172 Y. Xu, Z. Lin, X. Zhong, X. Huang, N. O. Weiss, Y. Huang and X. Duan, *Nat. Commun.*, 2014, **5**, 4554.
173 X. Tian, B. Xiao, X. Xu, L. Xu, Z. Liu, Z. Wang, M. Yan, Q. Wei and L. Mai, *Nano Res.*, 2016, **9**, 1012-1021.
174 J. Chang, S. Adhikari, T. H. Lee, B. Li, F. Yao, D. T. Pham, V. T. Le and Y. H. Lee, *Adv. Energy Mater.*, 2015, **5**, 1500003.
175 Q. Zhang, L. Huang, Q. Chang, W. Shi, L. Shen and Q. Chen, *Nanotechnology*, 2016, **27**, 105401.
176 M. Beidaghi and C. Wang, *Adv. Funct. Mater.*, 2012, **22**, 4501-4510.
177 G. Sun, J. Liu, X. Zhang, X. Wang, H. Li, Y. Yu, W. Huang, H. Zhang and P. Chen, *Angew. Chem.*, 2014, **126**, 12784-12788.
178 X. Zhao, B. M. Sanchez, P. J. Dobson and P. S. Grant, *Nanoscale*, 2011, **3**, 839-855.
179 W. Song, J. Zhu, B. Gan, S. Zhao, H. Wang, C. Li and J. Wang, *Small*, 2018, **14**, 1702249.
180 S. Liu, P. Gordiichuk, Z. S. Wu, Z. Liu, W. Wei, M. Wagner, N. Mohamed-Noriega, D. Wu, Y. Mai, A. Herrmann, K. Müllen and X. Feng, *Nat. Commun.*, 2015, **6**, 8817.
181 Z. Liu, S. Liu, R. Dong, S. Yang, H. Lu, A. Narita, X. Feng and K. Müllen, *Small*, 2017, **13**, 1603388.
182 Y. Liu, B. Zhang, Q. Xu, Y. Hou, S. Seyedin, S. Qin, G. G. Wallace, S. Beirne, J. M. Razal and J. Chen, *Adv. Funct. Mater.*, 2018, **0**, 1706592.
183 Z. S. Wu, K. Parvez, S. Li, S. Yang, Z. Liu, S. Liu, X. Feng and K. Müllen, *Adv. Mater.*, 2015, **27**, 4054-4061.
184 X. Tang, H. Zhou, Z. Cai, D. Cheng, P. He, P. Xie, D. Zhang and T. Fan, *ACS Nano*, 2018, **12**, 3502-3511.
185 X. Wang, B. D. Myers, J. Yan, G. Shekhawat, V. Dravid and P. S. Lee, *Nanoscale*, 2013, **5**, 4119-4122.
186 Z. Liu, X. Tian, X. Xu, L. He, M. Yan, C. Han, Y. Li, W. Yang and L. Mai, *Nano Res.*, 2017, **10**, 2471-2481.
187 H. Xu, X. Hu, H. Yang, Y. Sun, C. Hu and Y. Huang, *Adv. Energy Mater.*, 2015, **5**, 1401882.
188 X. Tian, M. Shi, X. Xu, M. Yan, L. Xu, A. Minhas-Khan, C. Han, L. He and L. Mai, *Adv. Mater.*, 2015, **27**, 7476-7482.
189 X. Ma, S. Feng, L. He, M. Yan, X. Tian, Y. Li, C. Tang, X. Hong and L. Mai, *Nanoscale*, 2017, **9**, 11765-11772.
190 X. Huang, H. Liu, X. Zhang and H. Jiang, *ACS Appl. Mater. Interfaces*, 2015, **7**, 27845-27852.
191 L. Sun, X. Wang, K. Zhang, J. Zou and Q. Zhang, *Nano Energy*, 2016, **22**, 11-18.
192 N. Kurra, C. Xia, M. N. Hedhili and H. N. Alshareef, *Chem. Commun.*, 2015, **51**, 10494-10497.
193 N. Kurra, N. A. Alhebshi and H. N. Alshareef, *Adv. Energy Mater.*, 2015, **5**, 1401303.
194 H. Haibo, P. Zhibin, F. Hongjin and Y. Changhui, *Small*, 2016, **12**, 3059-3069.
195 D. P. Dubal, D. Aradilla, G. Bidan, P. Gentile, T. J. S. Schubert, J. Wimberg, S. Sadki and P. Gomez-Romero, *Sci. Rep.*, 2015, **5**, 9771.
196 B. Shen, J. Lang, R. Guo, X. Zhang and X. Yan, *ACS Appl. Mater. Interfaces*, 2015, **7**, 25378-25389.
197 X. Shi, Z. Zeng, C. Liao, S. Tao, E. Guo, X. Long, X. Wang, D. Deng and Y. Dai, *J. Alloys Compd.*, 2018, **739**, 979-986.
198 C. Zhang, J. Xiao, L. Qian, S. Yuan, S. Wang and P. Lei, *J. Mater. Chem. A*, 2016, **4**, 9502-9510.
199 Y. Lin, Y. Gao and Z. Fan, *Adv. Mater.*, 2017, **29**, 1701736.
200 Y.-Q. Li, X.-M. Shi, X.-Y. Lang, Z. Wen, J.-C. Li and Q. Jiang, *Adv. Funct. Mater.*, 2016, **26**, 1830-1839.
201 C.-C. Liu, D.-S. Tsai, W.-H. Chung, K.-W. Li, K.-Y. Lee and Y.-S. Huang, *J. Power Sources*, 2011, **196**, 5761-5768.
202 Z. Su, C. Yang, B. Xie, Z. Lin, Z. Zhang, J. Liu, B. Li, F. Kang and C. P. Wong, *Energy Environ. Sci.*, 2014, **7**, 2652-2659.
203 J. Han, Y.-C. Lin, L. Chen, Y.-C. Tsai, Y. Ito, X. Guo, A. Hirata, T. Fujita, M. Esashi, T. Gessner and M. Chen, *Adv. Sci.*, 2015, **2**, 1500067.
204 Y. Yue, Z. Yang, N. Liu, W. Liu, H. Zhang, Y. Ma, C. Yang, J. Su, L. Li, F. Long, Z. Zou and Y. Gao, *ACS Nano*, 2016, **10**, 11249-11257.
205 N. Kurra, Q. Jiang and H. N. Alshareef, *Nano Energy*, 2015, **16**, 1-9.
206 S. C. Lee, U. M. Patil, S. J. Kim, S. Ahn, S.-W. Kang and S. C. Jun, *RSC Adv.*, 2016, **6**, 43844-43854.
207 C.-H. Chen, D.-S. Tsai, W.-H. Chung, K.-Y. Lee, Y.-M. Chen and Y.-S. Huang, *J. Power Sources*, 2012, **205**, 510-515.
208 H. Wu, K. Jiang, S. Gu, H. Yang, Z. Lou, D. Chen and G. Shen, *Nano Res.*, 2015, **8**, 3544-3552.
209 L. Li, J. Zhang, Z. Peng, Y. Li, C. Gao, Y. Ji, R. Ye, N. D. Kim, Q. Zhong, Y. Yang, H. Fei, G. Ruan and J. M. Tour, *Adv. Mater.*, 2016, **28**, 838-845.
210 W. Liu, X. Yan, J. Chen, Y. Feng and Q. Xue, *Nanoscale*, 2013, **5**, 6053-6062.
211 W.-W. Liu, Y.-Q. Feng, X.-B. Yan, J.-T. Chen and Q.-J. Xue, *Adv. Funct. Mater.*, 2013, **23**, 4111-4122.
212 T. M. Dinh, F. Mesnilgrente, V. Conédéra, N. A. Kyerematenga and D. Pech, *J. Electrochem. Soc.*, 2015, **162**, A2016-A2020.
213 C. Shen, X. Wang, S. Li, J. g. Wang, W. Zhang and F. Kang, *J. Power Sources*, 2013, **234**, 302-309.
214 N. Choudhary, C. Li, J. Moore, N. Nagaiah, L. Zhai, Y. Jung and J. Thomas, *Adv. Mater.*, 2017, **29**, 1605336.
215 S. E. Moosavifard, J. Shamsi, M. K. Altafi and Z. S. Moosavifard, *Chem. Commun.*, 2016, **52**, 13140-13143.
216 Q. Jiang, N. Kurra, C. Xia and H. N. Alshareef, *Adv. Energy Mater.*, 2017, **7**, 1601257.
217 S. Zheng, J. Ma, Z.-S. Wu, F. Zhou, Y. He, F. Kang, H.-M. Cheng and X. Bao, *Energy Environ. Sci.*, 2018, DOI: 10.1039/c8ee00855h.
218 H. Wang, H. Feng and J. Li, *Small*, 2014, **10**, 2165-2181.
219 Q. H. Wang, K. Kalantar-Zadeh, A. Kis, J. N. Coleman and M. S. Strano, *Nat. Nanotechnol.*, 2012, **7**, 699-712.
220 C. C. Mayorga-Martinez, J. G. S. Moo, B. Khezri, P. Song, A. C. Fisher, Z. Sofer and M. Pumera, *Adv. Funct. Mater.*, 2016, **26**, 6662-6667.
221 M. Acerce, D. Voiry and M. Chhowalla, *Nat. Nanotechnol.*, 2015, **10**, 313-318.
222 L. Cao, S. Yang, W. Gao, Z. Liu, Y. Gong, L. Ma, G. Shi, S. Lei, Y. Zhang, S. Zhang, R. Vajtai and P. M. Ajayan, *Small*, 2013, **9**, 2905-2910.

223 X. Geng, Y. Zhang, Y. Han, J. Li, L. Yang, M. Benamara, L. Chen and H. Zhu, *Nano Lett.*, 2017, **17**, 1825-1832.
224 M. Chhowalla, H. S. Shin, G. Eda, L.-J. Li, K. P. Loh and H. Zhang, *Nat. Chem.*, 2013, **5**, 263-275.
225 J. Feng, X. Sun, C. Wu, L. Peng, C. Lin, S. Hu, J. Yang and Y. Xie, *J. Am. Chem. Soc.*, 2011, **133**, 17832-17838.
226 J. Wu, J. Peng, Z. Yu, Y. Zhou, Y. Guo, Z. Li, Y. Lin, K. Ruan, C. Wu and Y. Xie, *J. Am. Chem. Soc.*, 2018, **140**, 493-498.
227 X. Zhang, Z. Lai, C. Tan and H. Zhang, *Angew. Chem. Int. Ed.*, 2016, **55**, 8816-8838.
228 M. R. Lukatskaya, O. Mashtalir, C. E. Ren, Y. Dall'Agnese, P. Rozier, P. L. Taberna, M. Naguib, P. Simon, M. W. Barsoum and Y. Gogotsi, *Science*, 2013, **341**, 1502-1505.
229 M. Ghidiu, M. R. Lukatskaya, M.-Q. Zhao, Y. Gogotsi and M. W. Barsoum, *Nature*, 2014, **516**, 78-81.
230 B. Anasori, M. R. Lukatskaya and Y. Gogotsi, *Nat. Rev. Mater.*, 2017, **2**, 16098.
231 O. Mashtalir, M. Naguib, V. N. Mochalin, Y. Dall'Agnese, M. Heon, M. W. Barsoum and Y. Gogotsi, *Nat. Commun.*, 2013, **4**, 1716.
232 M. Naguib, V. N. Mochalin, M. W. Barsoum and Y. Gogotsi, *Adv. Mater.*, 2014, **26**, 992-1005.
233 B. Anasori, Y. Xie, M. Beidaghi, J. Lu, B. C. Hosler, L. Hultman, P. R. C. Kent, Y. Gogotsi and M. W. Barsoum, *ACS Nano*, 2015, **9**, 9507-9516.
234 M. Naguib, O. Mashtalir, J. Carle, V. Presser, J. Lu, L. Hultman, Y. Gogotsi and M. W. Barsoum, *ACS Nano*, 2012, **6**, 1322-1331.
235 N. Kurra, B. Ahmed, Y. Gogotsi and H. N. Alshareef, *Adv. Energy Mater.*, 2016, **6**, 1601372.
236 B.-S. Shen, H. Wang, L.-J. Wu, R.-S. Guo, Q. Huang and X.-B. Yan, *Chin. Chem. Lett.*, 2016, **27**, 1586-1591.
237 M. Naguib, J. Come, B. Dyatkin, V. Presser, P.-L. Taberna, P. Simon, M. W. Barsoum and Y. Gogotsi, *Electrochem. Commun.*, 2012, **16**, 61-64.
238 H. Li, Y. Hou, F. Wang, M. R. Lohe, X. Zhuang, L. Niu and X. Feng, *Adv. Energy Mater.*, 2017, **7**, 1601847.
239 Z. Ling, C. E. Ren, M.-Q. Zhao, J. Yang, J. M. Giammarco, J. Qiu, M. W. Barsoum and Y. Gogotsi, *Proc. Natl. Acad. Sci. USA*, 2014, **111**, 16676-16681.
240 M. Q. Zhao, X. Xie, C. E. Ren, T. Makaryan, B. Anasori, G. Wang and Y. Gogotsi, *Adv. Mater.*, 2017, **29**, 1702410.
241 M. Naguib, J. Halim, J. Lu, K. M. Cook, L. Hultman, Y. Gogotsi and M. W. Barsoum, *J. Am. Chem. Soc.*, 2013, **135**, 15966-15969.
242 C. F. Zhang, M. P. Kremer, A. Seral-Ascaso, S. H. Park, N. McEvoy, B. Anasori, Y. Gogotsi and V. Nicolosi, *Adv. Funct. Mater.*, 2018, **28**, 1705506.
243 J. Wang, J. Tang, B. Ding, V. Malgras, Z. Chang, X. Hao, Y. Wang, H. Dou, X. Zhang and Y. Yamauchi, *Nat. Commun.*, 2017, **8**, 15717.
244 M. Xu, S. Lei, J. Qi, Q. Dou, L. Liu, Y. Lu, Q. Huang, S. Shi and X. Yan, *ACS Nano*, 2018, **12**, 3733-3740.
245 C. Chen, M. Boota, P. Urbankowski, B. Anasori, L. Miao, J. Jiang and Y. Gogotsi, *J. Mater. Chem. A*, 2018, **6**, 4617-4622.
246 C. Chen, M. Boota, X. Xie, M. Zhao, B. Anasori, C. E. Ren, L. Miao, J. Jiang and Y. Gogotsi, *J. Mater. Chem. A*, 2017, **5**, 5260-5265.
247 M. R. Lukatskaya, S. Kota, Z. F. Lin, M. Q. Zhao, N. Shpigel, M. D. Levi, J. Halim, P. L. Taberna, M. Barsoum, P. Simon and Y. Gogotsi, *Nat. Energy*, 2017, **2**, 17105.
248 S. Dang, Q.-L. Zhu and Q. Xu, *Nat. Rev. Mater.*, 2017, **3**, 17075.
249 A. K. Mandal, J. Mahmood and J.-B. Baek, *ChemNanoMat*, 2017, **3**, 373-391.
250 J. Liu and C. Woll, *Chem. Soc. Rev.*, 2017, **46**, 5730-5770.
251 S. K. Das, K. Bhunia, A. Mallick, A. Pradhan, D. Pradhan and A. Bhaumik, *Microporous Mesoporous Mater.*, 2018, **266**, 109-116.
252 W. H. Li, K. Ding, H. R. Tian, M. S. Yao, B. Nath, W. H. Deng, Y. Wang and G. Xu, *Adv. Funct. Mater.*, 2017, **27**, 1702067.
253 C. Yang, K. S. Schellhammer, F. Ortmann, S. Sun, R. Dong, M. Karakus, Z. Mics, M. Löffler, F. Zhang, X. Zhuang, E. Cánovas, G. Cuniberti, M. Bonn and X. Feng, *Angew. Chem. Int. Ed.*, 2017, **56**, 3920-3924.
254 Q. Jiang, N. Kurra and H. N. Alshareef, *Adv. Funct. Mater.*, 2015, **25**, 4976-4984.
255 K. Guo, Y. Wan, N. Yu, L. Hu, T. Zhai and H. Li, *Energy Storage Mater.*, 2018, **11**, 144-151.
256 H. U. Lee and S. W. Kim, *J. Mater. Chem. A*, 2017, **5**, 13581-13590.
257 C. Shen, X. Wang, W. Zhang and F. Kang, *J. Power Sources*, 2011, **196**, 10465-10471.
258 S.-K. Kim, H.-J. Koo, A. Lee and P. V. Braun, *Adv. Mater.*, 2014, **26**, 5108-5112.
259 L. Li, Z. Lou, W. Han, D. Chen, K. Jiang and G. Shen, *Adv. Mater. Technol.*, 2017, **2**, 1600282.
260 S. Li, X. Wang, H. Xing and C. Shen, *J. Micromech. Microeng.*, 2013, **23**, 114013.
261 R. Sharma, C. C. B. Bufon, D. Grimm, R. Sommer, A. Wollatz, J. Schadewald, D. J. Thurmer, P. F. Siles, M. Bauer and O. G. Schmidt, *Adv. Energy Mater.*, 2014, **4**, 1301631.
262 H. Ji, Y. Mei and O. G. Schmidt, *Chem. Commun.*, 2010, **46**, 3881-3883.
263 J. Lin, C. Zhang, Z. Yan, Y. Zhu, Z. Peng, R. H. Hauge, D. Natelson and J. M. Tour, *Nano Lett.*, 2013, **13**, 72-78.
264 W. Yang, L. He, X. C. Tian, M. Y. Yan, H. Yuan, X. B. Liao, J. S. Meng, Z. M. Hao and L. Q. Mai, *Small*, 2017, **13**, 1700639.
265 D. Qi, Z. Liu, Y. Liu, W. R. Leow, B. Zhu, H. Yang, J. Yu, W. Wang, H. Wang, S. Yin and X. Chen, *Adv. Mater.*, 2015, **27**, 5559-5566.
266 Y. Zheng, Y. Yang, S. Chen and Q. Yuan, *CrystEngComm*, 2016, **18**, 4218-4235.
267 M. Ye, Z. Zhang, Y. Zhao and L. Qu, *Joule*, 2018, **2**, 245-268.
268 L. Zhang, M. Liao, L. Bao, X. Sun and H. Peng, *Small Methods*, 2017, **1**, 1700211.
269 Y. Huang, M. Zhu, Y. Huang, Z. Pei, H. Li, Z. Wang, Q. Xue and C. Zhi, *Adv. Mater.*, 2016, **28**, 8344-8364.
270 X. Yu, H. Cheng, M. Zhang, Y. Zhao, L. Qu and G. Shi, *Nat. Rev. Mater.*, 2017, **2**, 17046.
271 G. Lee, S. K. Kang, S. M. Won, P. Gutruf, Y. R. Jeong, J. Koo, S. S. Lee, J. A. Rogers and J. S. Ha, *Adv. Energy Mater.*, 2017, **7**, 1700157.
272 D. W. Zhao, C. J. Chen, Q. Zhang, W. S. Chen, S. X. Liu, Q. W. Wang, Y. X. Liu, J. Li and H. P. Yu, *Adv. Energy Mater.*, 2017, **7**, 1700739.
273 S. S. Lee, K. H. Choi, S. H. Kim and S. Y. Lee, *Adv. Funct. Mater.*, 2018, **28**, 1705571.
274 Y. Huang, M. Zhong, Y. Huang, M. Zhu, Z. Pei, Z. Wang, Q. Xue, X. Xie and C. Zhi, *Nat. Commun.*, 2015, **6**, 10310.
275 Y. Yue, N. Liu, Y. Ma, S. Wang, W. Liu, C. Luo, H. Zhang, F. Cheng, J. Rao, X. Hu, J. Su and Y. Gao, *ACS Nano*, 2018, **12**, 4224-4232.
276 J. Wang, L. Zhang, L. Yu, Z. Jiao, H. Xie, X. W. Lou and X. W. Sun, *Nat. Commun.*, 2014, **5**, 4921.
277 F. Wang, H. Yang, J. Zhang, P. Zhang, G. Wang, X. Zhuang, G. Cuniberti and X. Feng, *Adv. Mater.*, 2018, **30**, 1800028.
278 J. Deng, Y. Zhang, Y. Zhao, P. Chen, X. Cheng and H. Peng, *Angew. Chem. Int. Ed.*, 2015, **54**, 15419-15423.
279 M. Zhu, Z. Wang, H. Li, Y. Xiong, Z. Liu, Z. Tang, Y. Huang, A. Rogach and C. Zhi, *Energy Environ. Sci.*, 2018, DOI: 10.1039/C8EE00590G.
280 X. Wang, B. Liu, R. Liu, Q. Wang, X. Hou, D. Chen, R. Wang and G. Shen, *Angew. Chem.*, 2014, **126**, 1880-1884.

281 Z. Chen, P.-C. Hsu, J. Lopez, Y. Li, J. W. F. To, N. Liu, C. Wang, Sean C. Andrews, J. Liu, Y. Cui and Z. Bao, *Nat. Energy*, 2016, **1**, 15009.
282 Y. Yang, D. Yu, H. Wang and L. Guo, *Adv. Mater.*, 2017, **29**, 1703040.
283 H. Yang, W. R. Leow and X. Chen, *Adv. Mater.*, 2018, DOI: 10.1002/adma.201704347, 1704347.
284 P. Zhang, J. Wang, W. Sheng, F. Wang, J. Zhang, F. Zhu, X. Zhuang, R. Jordan, O. G. Schmidt and X. Feng, *Energy Environ. Sci.*, 2018, DOI: 10.1039/C8EE00365C.
285 P. Zhang, F. Zhu, F. Wang, J. Wang, R. Dong, X. Zhuang, O. G. Schmidt and X. Feng, *Adv. Mater.*, 2017, **29**, 1604491.
286 J. Maeng, C. Meng and P. P. Irazoqui, *Biomed. Microdevices*, 2015, **17**, 7.
287 Z. Wang, A. Chen, R. Winslow, D. Madan, R. C. Juang, M. Nill, J. W. Evans and P. K. Wright, *J. Micromech. Microeng.*, 2012, **22**, 094001.
288 C. W. Shen, S. X. Xu, Y. X. Xie, M. Sanghadasa, X. H. Wang and L. W. Lin, *J. Microelectromech. Syst.*, 2017, **26**, 949-965.
289 B. Luo, D. Ye and L. Wang, *Adv. Sci.*, 2017, **4**, 1700104.
290 K. U. Laszczyk, K. Kobashi, S. Sakurai, A. Sekiguchi, D. N. Futaba, T. Yamada and K. Hata, *Adv. Energy Mater.*, 2015, **5**, 1500741.
291 F. Albano, Y. S. Lin, D. Blaauw, D. M. Sylvester, K. D. Wise and A. M. Sastry, *J. Power Sources*, 2008, **185**, 1524-1532.
292 S. Qin, Q. Zhang, X. Yang, M. Liu, Q. Sun and Z. L. Wang, *Adv. Energy Mater.*, 2018, **0**, 1800069.
293 Y. Zhong, X. Xia, W. Mai, J. Tu and H. J. Fan, *Adv. Mater. Technol.*, 2017, **2**, 1700182.
294 X. Liu, S. Chen, J. Pu and X. Wang, *J. Microelectromech. Syst.*, 2016, **25**, 929-936.
295 S. Siddiqui, D.-I. Kim, L. T. Duy, M. T. Nguyen, S. Muhammad, W.-S. Yoon and N.-E. Lee, *Nano Energy*, 2015, **15**, 177-185.
296 J. Xu, Y. Chen and L. Dai, *Nat. Commun.*, 2015, **6**, 8103.
297 M. Zhu, Y. Huang, Y. Huang, H. Li, Z. Wang, Z. Pei, Q. Xue, H. Geng and C. Zhi, *Adv. Mater.*, 2017, **29**, 1605137.
298 X. Liu, K. Zhao, Z. L. Wang and Y. Yang, *Adv. Energy Mater.*, 2017, **7**, 1701629.
299 Q. Jiang, C. S. Wu, Z. J. Wang, A. C. Wang, J. H. He, Z. L. Wang and H. N. Alshareef, *Nano Energy*, 2018, **45**, 266-272.
300 X. Wang, Y. Yin, F. Yi, K. Dai, S. Niu, Y. Han, Y. Zhang and Z. You, *Nano Energy*, 2017, **39**, 429-436.
301 Z. Lou, Li, L. Wang and G. Shen, *Small*, 2017, **13**, 1701791.
302 L. Liu, Z. Niu and J. Chen, *Nano Res.*, 2017, **10**, 1524-1544.
303 B. Luca Giacomo, B. Andrea, P. Paolo and M. Paolo, *Flex. Print. Electron.*, 2017, **2**, 025002.
304 S. Xu, Y. Dall'Agnese, G. Wei, C. Zhang, Y. Gogotsi and W. Han, *Nano Energy*, 2018, **50**, 479-488.
305 D. Kim, J. Yun, G. Lee and J. S. Ha, *Nanoscale*, 2014, **6**, 12034-12041.
306 Y. S. Moon, D. Kim, G. Lee, S. Y. Hong, K. K. Kim, S. M. Park and J. S. Ha, *Carbon*, 2015, **81**, 29-37.
307 C. Chen, J. Cao, X. Wang, Q. Lu, M. Han, Q. Wang, H. Dai, Z. Niu, J. Chen and S. Xie, *Nano Energy*, 2017, **42**, 187-194.
308 D. Kim, D. Kim, H. Lee, Y. R. Jeong, S.-J. Lee, G. Yang, H. Kim, G. Lee, S. Jeon, G. Zi, J. Kim and J. S. Ha, *Adv. Mater.*, 2016, **28**, 748-756.
309 J. Yun, Y. Lim, H. Lee, G. Lee, H. Park, S. Y. Hong, S. W. Jin, Y. H. Lee, S. S. Lee and J. S. Ha, *Adv. Funct. Mater.*, 2017, **27**, 1700135.
310 J. Yun, Y. Lim, G. N. Jang, D. Kim, S.-J. Lee, H. Park, S. Y. Hong, G. Lee, G. Zi and J. S. Ha, *Nano Energy*, 2016, **19**, 401-414.
311 J. Ye, H. Tan, S. Wu, K. Ni, F. Pan, J. Liu, Z. Tao, Y. Qu, H. Ji, P. Simon and Y. Zhu, *Adv. Mater.*, 2018, **0**, e1801384.
312 L. Li, C. W. Fu, Z. Lou, S. Chen, W. Han, K. Jiang, D. Chen and G. Z. Shen, *Nano Energy*, 2017, **41**, 261-268.
313 R. S. Guo, J. T. Chen, B. J. Yang, L. Y. Liu, L. J. Su, B. S. Shen and X. B. Yan, *Adv. Funct. Mater.*, 2017, **27**, 1702394.